

Diagenesis and reservoir properties of Cretaceous-Lower Tertiary sandstones: the GANT-1 well, western Nuussuaq, central West Greenland

Thomas Kierkegaard



**Diagenesis and reservoir properties of Cretaceous-Lower
Tertiary sandstones: the GANT-1 well, western Nuussuaq,
central West Greenland**

Thomas Kierkegaard

Contents

Introduction	3
Depositional environment and stratigraphy	4
Methods	7
Sandstones	8
Detrital components	8
Diagenetic alterations	12
Campanian diagenetic stage: concretionary zones	12
Post-Campanian diagenetic stage	18
Early diagenetic events	18
Late diagenetic events	19
Microfractures	22
Mudstones	23
Intrusion-related diagenetic effects	26
Diagenetic model	27
Campanian diagenetic stage	27
Post-Campanian diagenetic stage	29
Reservoir conditions	32
Conclusions	34
References	35
Plates	38

Introduction

The main purpose of this study is to describe the diagenetic alterations occurring in the Cretaceous to Lower Paleocene sedimentary succession of the GANT#1 well, and to determine the diagenetic and detrital factors which control present porosity and permeability.

The GANT#1 well is located on north-western Nuussuaq, central West Greenland (Fig. 1). The West Greenland margin is a continental margin subdivided into linked basins where Cretaceous to Lower Tertiary and probably older sediments have been deposited (Rolle 1985; Chalmers *et al.* 1993). In the Nuussuaq area these sediments are overlain by a succession of Early Tertiary basaltic volcanic rocks which reaches a combined thickness of around 2–2.5 km (Larsen *et al.* in press). The GANT#1 well is situated in the Tunorsuaq valley about 11 km east of the Itilli valley and 6 km south-west of Kangilia on the north coast of Nuussuaq (Fig. 1). Below 35 m of Quaternary overburden the well penetrates about 865 meters of marine slope deposits of Paleocene and Cretaceous age (Dam 1996). At a stratigraphic level less than 200 m above the well location both sides of the Tunorsuaq valley are flanked by altered, basaltic pillow breccias belonging to the Lower Tertiary volcanic succession. GANT#1 was drilled during summer 1995 together with two other wells, GANE#1 and GANK#1 on the south-western coast of Nuussuaq (Fig. 1; Dam 1996).

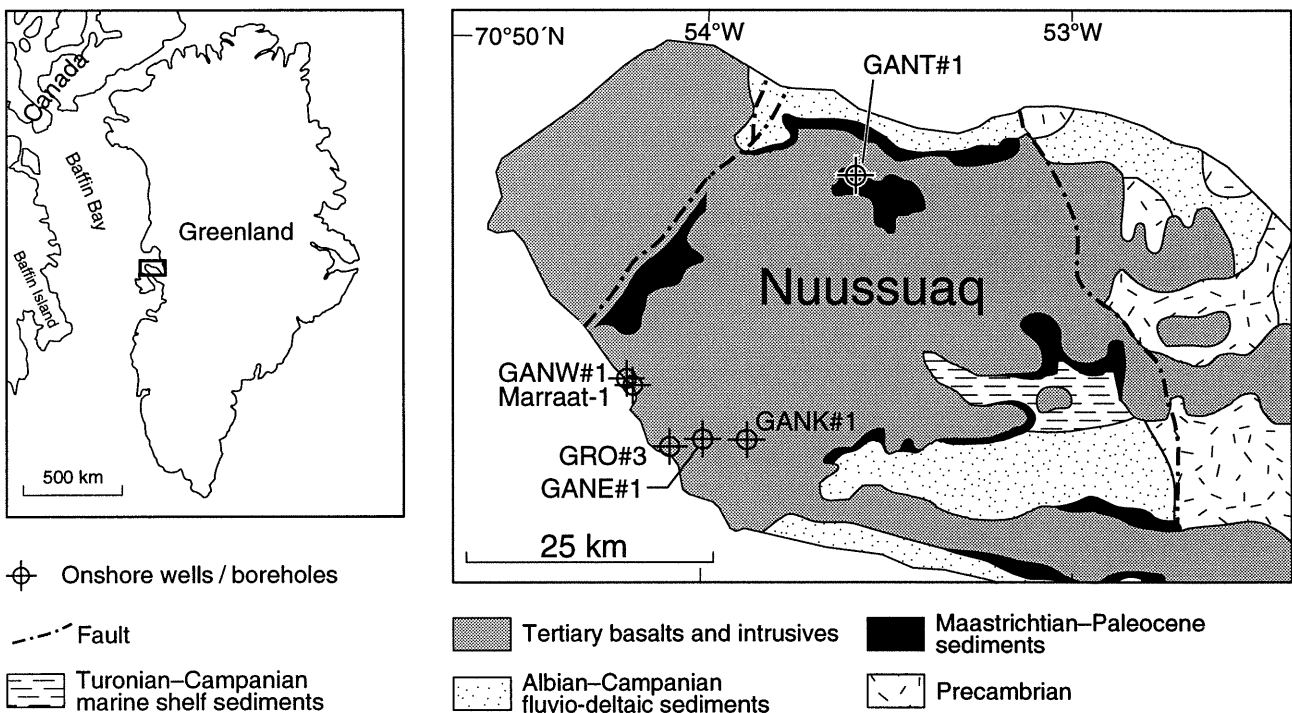


Figure 1. Simplified geological map of western Nuussuaq, showing position of the GANT#1 well.

Depositional environment and stratigraphy

The Cretaceous to lower Tertiary sedimentary succession penetrated in the 901 m deep GANT#1 well was deposited in a marine slope environment and is dominated by amalgamated turbidite channel sandstones and conglomerates, mass flow deposits and thinly interbedded interchannel turbidite sandstone and mudstone (Fig. 2; Dam 1996). Six facies associations are identified: 1) thinly interbedded sandstone and mudstone, 2) massive sandy mudstone, 3) massive muddy sandstone, 4) amalgamated sandstone and conglomerate, 5) single graded sandstone beds, and 6) slumped beds. The vertical facies development suggests that deposition took place on a fault-controlled slope in canyons, major and small distributary feeder channels, small turbidite lobes and interdistributary channel areas. Sandstones of facies association 4 are interpreted as channel sandstones, and thinly interbedded sandstones and mudstones of facies association 1 are interpreted as interchannel deposits from waning, low density turbidite currents and suspension (Dam 1996).

The sediments of the GANT#1 core are dated by a palynological screening as Early Campanian (Late Cretaceous) to early Danian (Early Paleocene) (Nøhr-Hansen 1997). Based on lithostratigraphy, the uppermost 525 m of the GANT#1 well are correlated with outcrops on the north coast of Nuusuaq (Kangilia and Annertuneq). The 130 m thick succession of amalgamated conglomerate and sandstone which occurs above 255.85 m in the GANT#1 well is correlated with a major conglomeratic submarine canyon fill (the 'Conglomerate Member' of Rosenkrantz 1970).

A major unconformity is identified at 255.85 m which separates Late Campanian slope deposits from overlying Maastrichtian–Paleocene amalgamated conglomerates and sandstones (Dam 1996; Nøhr-Hansen 1997; Nøhr-Hansen & Dam 1997).

The sedimentary succession in the GANT#1 well is intersected by 15 intrusions varying in thickness from 0.55 m to 4.4 m. Of these, 10 intersect intervals with sandstones or conglomerates (Fig. 2).

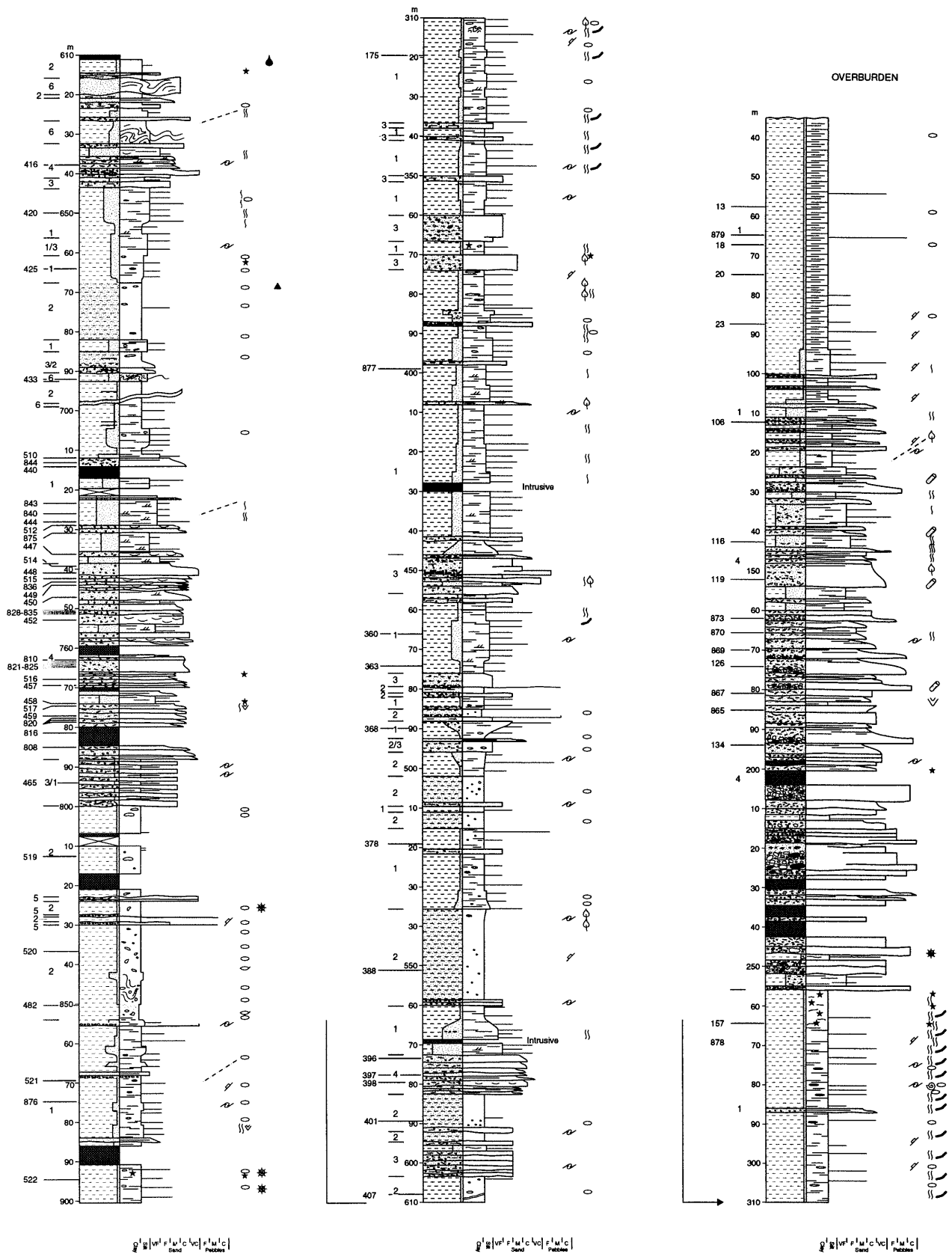



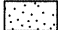

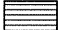


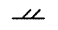
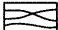





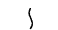
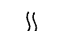
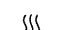









Figure 2. Sedimentological log of the GANT#1 well (GGU no. 439101) showing position of samples. Legend on next page (after Dam 1996).

LEGEND

Facies associations

- 1 Thinly interbedded sandstone and mudstone
 - 2 Massive sandy mudstone
 - 3 Massive muddy sandstone
 - 4 Amalgamated sandstones and conglomerates
 - 5 Single graded sandstone beds
 - 6 Slumped beds
-  Volcanic sills
-  Clay and siltstone
-  Muddy sandstone/sandy mudstone
-  Sandstone
-  Sandstone with pebbles and mudstone clasts
-  Parallel lamination
-  Slumping
-  Disturbed bedding
-  Cross-lamination
-  Bioturbation
-  Concretions
-  Ammonite
-  Bivalve
-  Plant and wood fragments
-  Logs
-  Weakly bioturbated
-  Moderately bioturbated
-  Heavily bioturbated
-  *Planolites* isp.
-  *Helminthopsis horizontalis*
-  Escape burrows
-  Fractures
-  Pyrite
-  Oil
-  Gas

Methods

The samples were analysed with a standard optical polarisation microscope, scanning electron microscopy (SEM) and X-ray diffractometry (XRD). Most thin sections were stained with Alizarin Red and potassium ferricyanide for carbonate identification. The thin sections were produced at the University of Aarhus and at the University of Copenhagen.

Scanning electron microscopy was carried out at the Geological Survey of Denmark and Greenland (GEUS) on a Phillips XLS 40 with a Noran Instruments Voyager 2.7 EDX equipment.

XRD analysis were carried out partly at the University of Aarhus (Philips 3710 based) using CuK α radiation and partly at GEUS (Philips 1050/80) using CoK α radiation. The study performed at GEUS was done on oriented mounts for clay mineral analysis prepared from the <0.2 mm and the 0.2–2 mm size fractions by the pipette method and included (a) saturation with MgCl $_2$, (b) saturation with KCl, (c) heating with KCl to 300°C, (d) glycerol solvation of the <0.2mm size fraction, (e) ethylene-glycol solvation with the sample subjected to vapour at 60°C for 3 days. Samples were dissolved for carbonates and for iron compounds, but not for organic material.

Chemical compositions of authigenic carbonate and detrital feldspar were analysed with an electron microprobe (Jeol JXA 8600) at the University of Aarhus.

Oxygen and carbon isotope data were analysed by the GMS laboratory, Department of Geology, University of Bergen, Norway.

Sandstones

Detrital components

The grain size of the analysed sandstone samples varies from fine to coarse. The bulk of the Campanian sandstones below the unconformity at 255.85 m are medium- to coarse-grained, whereas most of the overlying sandstones are coarse-grained. It is estimated, that the sandstones are generally poorly sorted but that sorting is slightly better above the unconformity where the coarse-grained sandstones contain relatively little, if any, detrital clay. The rounding is in general not possible to estimate due to alteration of the detrital grains by pressure solution and overgrowth, but some well rounded grains have remained intact. Quartz (62–96%) and feldspar (1–28%) form the main detrital constituents accompanied by lithic fragments of various composition (<7%). Micaceous and plant debris generally constitute less than 5% but plant debris may at certain levels form major constituents amounting to 13%. Glauconite, zircon, tourmaline, Ti-oxides, and opaques all occur in trace amounts (Table 1). Constituents referred to as Mg-siderite aggregates are mainly composed of diagenetic microcrystalline Mg-siderite. The aggregates generally constitute less than 10% by volume but in a few samples they form as much as 40%. They are interpreted as intraformational clasts and are thus excluded from the lithic fragment assemblage used to classify the sandstone since they are not part of the detritus sourced from the hinterland. Most of the sandstones thus classify as subarkoses (Figs 3a–c) according to the classification system by Folk (1968).

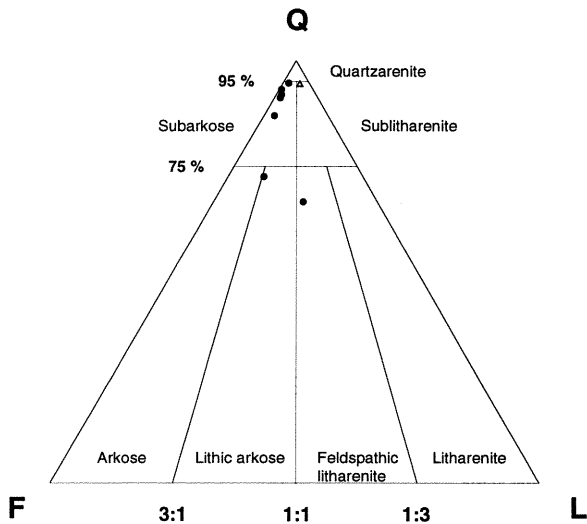
Quartz. Quartz is the main detrital component and constitutes 62–96% of the framework detritals. Polycrystalline grains are in many samples a significant constituent with the mono-Q/poly-Q ratio amounting up to 3. The polycrystalline grains are mainly metamorphic but some may be of granitic origin. Most of the grains have undulose extinction. Multi-cycle grains with rounded overgrowths are present in minor amounts.

A slight compositional differences has been observed for channel sandstones above and below the unconformity at 255.85 m. Above the unconformity, channel sandstones contain relatively more quartz and lithic fragments than below the unconformity (Fig 3a–c), and interchannel sandstones interbedded with mudstone (facies association 1) are more rich in quartz than channel sandstones (facies association 4) (Fig 3b, c). No changes in the Q-F-L compositions have been observed in the vicinity of intrusions.

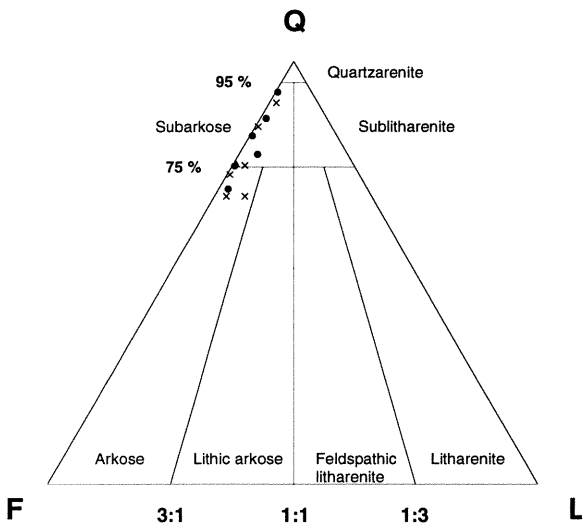
Feldspar. Feldspar constitutes 1–28% of the framework detritals (Table 1) and it is estimated that plagioclase and microcline constitute equal amounts. Each thin section contains strongly sericitised as well as fresh feldspar grains. Most K-feldspar displays microcline twinning and only minor amounts are untwinned or perthitic. Microprobe analyses revealed that plagioclase is present as albite, oligoclase and anorthite, and that K-feldspar contains some Na (Fig. 4). A representative range of different compositions is tabulated in Table 2. Preliminary analysis with EDX indicates that the feldspars do not contain Ba. During microprobe analysis oligoclase was never found in samples from the sandstone succession above the unconformity.

Table 1. Framework detrital percentage of pointcounted samples together with calculated quartz/feldspar-ratios. It is also indicated whether the samples are from within a concretionary zone or from less uncemented sandstones. The line between sample 134 and 863 separates Campanian and Upper Maastrichtian–Paleocene sediments. Data are based on 200 counts in each thin section.

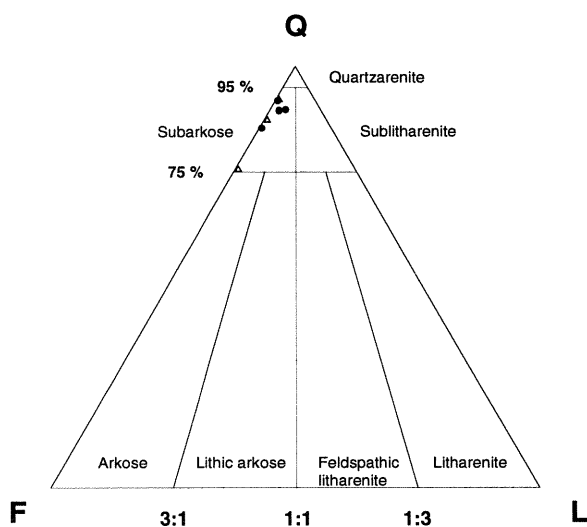
Sample number	Mono-Q	Poly-Q	Total quartz	Feldspar	Rock fragments	Mudstone clasts	Chert	Mica	Heavy minerals	Plant debris	Q/F ratio	Concretionary zone
116	65.9	7.6	73.5	19.7	0.0	6.7	0.0	0.0	0.0	0.0	3.7	÷
873	82.6	10.3	92.9	5.8	0.6	0.6	0.0	0.0	0.0	0.0	16.0	÷
870	81.6	6.4	88.0	9.6	0.8	1.6	0.0	0.0	0.0	0.0	9.2	÷
869	70.0	22.1	92.1	5.7	1.4	0.7	0.0	0.0	0.0	0.0	16.1	÷
126	62.8	4.9	67.6	14.2	0.4	16.6	1.2	0.0	0.0	0.0	4.8	÷
867	84.4	9.7	94.2	5.8	0.0	0.0	0.0	0.0	0.0	0.0	16.1	÷
865	77.0	18.7	95.7	1.4	2.2	0.7	0.0	0.0	0.0	0.0	66.5	÷
134	77.1	14.0	91.1	3.2	1.9	2.5	0.0	1.3	0.0	0.0	28.6	÷
863	55.8	5.8	61.5	27.9	1.9	0.0	1.9	2.9	0.0	3.8	2.2	+
858	63.3	8.3	71.6	20.2	1.8	0.0	0.0	1.8	0.0	4.6	3.5	+
857	66.9	5.0	71.9	21.5	0.8	0.0	0.0	1.7	0.0	4.1	3.3	÷
853	75.7	13.2	89.0	5.9	0.0	0.0	0.0	1.5	0.0	3.7	15.1	÷
851	59.5	7.2	66.7	24.3	3.6	0.0	1.8	0.0	0.0	3.6	2.7	+
420	68.5	6.9	75.4	5.4	0.0	0.8	1.5	3.8	0.0	13.1	14.0	÷
510	66.0	20.9	86.9	10.5	0.7	0.0	0.0	0.7	0.0	1.3	8.3	÷
844	72.2	1.6	73.8	22.2	0.0	0.0	0.0	0.8	0.0	3.2	3.3	+
440	78.9	10.9	89.8	6.3	0.0	0.0	0.0	2.3	0.0	1.6	14.4	+
444	72.7	17.4	90.2	6.8	0.0	0.0	0.0	2.3	0.0	0.8	13.2	÷
512	74.0	11.6	85.6	6.8	0.7	1.4	0.0	2.7	0.7	2.1	12.5	÷
447	77.7	5.4	83.1	13.1	0.0	0.0	0.0	1.5	0.0	2.3	6.4	÷
834	68.4	13.8	82.2	15.1	1.3	0.0	0.0	0.7	0.0	0.7	5.4	÷
832	62.2	24.4	86.6	6.7	0.8	0.8	0.0	1.7	0.0	3.4	12.9	+
452	79.5	6.8	86.3	11.6	0.0	0.7	0.0	0.7	0.0	0.7	7.4	÷
516	60.9	10.1	71.0	15.9	0.0	2.9	0.0	5.1	0.0	5.1	4.5	÷
457	73.9	4.3	78.3	12.2	0.9	0.0	0.0	1.7	0.9	6.1	6.4	+
517	69.1	0.7	69.8	27.3	0.0	1.4	0.0	0.7	0.0	0.7	2.6	÷
819	61.2	3.9	65.1	22.5	0.0	0.0	0.0	1.6	0.0	10.9	2.9	+
818	76.2	3.5	79.7	16.1	0.0	0.0	0.0	1.4	0.0	2.8	5.0	÷



A: Post-Campanian channel sandstone
near intrusion



B: Campanian channel sandstone
concretionary zone
near intrusion



C: Campanian interchannel sandstone
near intrusion

Figure 3. Sandstone classification according to the system by Folk (1968). Q: quartz (excluding chert), F: feldspar and rock fragments, L: lithic fragments include mudstone clasts and chert. Mg-siderite aggregates are not included in the classification.

Table 2. Oxide results, wt-%, for a representative range of composition of detrital feldspar grains.

	1	2	3	4	5	6	7	8	9
SiO ₂	67.60	70.39	63.29	70.49	64.55	64.53	64.33	63.97	64.16
Al ₂ O ₃	20.41	19.81	23.68	20.59	22.13	18.73	18.20	18.39	18.57
FeO	0.13	0.04	0.01	0.15	0.07	0.04	0.06	0.13	0.00
CaO	0.65	0.00	4.71	0.67	3.18	0.12	0.11	0.34	0.14
Na ₂ O	11.20	10.33	8.91	7.58	9.69	0.40	0.58	0.38	0.66
K ₂ O	0.19	0.03	0.07	1.08	0.31	16.32	16.92	16.85	16.85
Total	100.18	100.60	100.67	100.56	99.93	100.14	100.20	100.06	100.38

1: Plagioclase, sample 512; 2: Albitised feldspar, sample 119; 3: Oligoclase, sample 416; 4: Anorthoclase, sample 416; 5: Oligoclase, sample 459; 6: K-feldspar, sample 119; 7: K-feldspar, sample 134; 8: K-feldspar, sample 398; 9: K-feldspar, sample 512.

Lithic fragments. Lithic fragments constitute less than 7% of the framework detritals except in one sample which contains 18% due to a high content of mudstone clasts. The lithic fragments are in general dominated by mudstone clasts; chert, polymineralic metamorphic or granitic rock fragments are less abundant (Table 1). Polymineralic rock fragments consist of quartz, feldspar and mica (Plate 1.1).

Deformation due to compaction is the most significant alteration of the lithic fragments. Clay clasts are squeezed by surrounding grains which develop a characteristic flame structured pseudomatrix (Plate 1.2; cf. Dickinson 1970). Chert, which is most easily differentiated from polycrystalline quartz by its yellow-brownish colour (Plate 2.1), is altered by pressure solution in a similar fashion to monocrystalline quartz grains. The original amount of polymineralic fragments may have been higher, but it was not possible to identify, and thereby quantify, disintegrated rock fragments.

Micas. Muscovite and strongly altered biotite constitute less than 4% of the framework detritals. Campanian sandstones are richer in mica than the overlying sandstones (Table 1). The micas are altered by dissolution and by mechanic deformation against more rigid quartz and feldspar grains.

Dissolution parallel to cleavage planes is more severe in biotite than in muscovite. The biotite has retained a weak pleochroism.

Heavy minerals. Zircon, tourmaline (with a strong, green pleochroism), Ti-oxides, and opaques all occur in trace amounts. Zircon, which is the most abundant heavy mineral, is often fractured along internal zonations.

Plant debris. In the studied Campanian sandstones plant debris generally constitutes less than 5% whereas sandstones overlying the unconformity only contain minor amounts (Table 1). The plant debris is tabular in shape and often microporous (Plate 2.2).

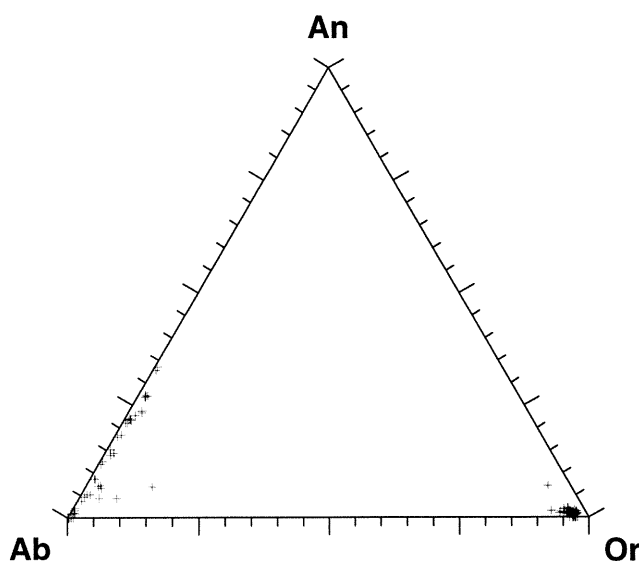


Figure 4. Feldspar composition in mole-% albite-anorthite-orthoclase.

Glauconite. Glauconite grains are very rare and have sizes similar to other framework detritals. Some grains are rounded but most are strongly altered by dissolution or mixed-layer clay replacement. The original amount of glauconite is indeterminable.

Diagenetic alterations

The unconformity recognised at 255.85 m can be traced throughout the Nuussuaq Basin (Dam & Sønderholm 1998). This unconformity is interpreted to separate two distinct diagenetic stages of which the first only affects the Campanian deposits and the second the combined Campanian–Paleocene succession.

Campanian diagenetic stage: concretionary zones

This stage is characterised by initial growth of apatite and pyrite followed by siderite, quartz, mixed-layer clay, dissolution of feldspar and finally by cementation with ferroan carbonate which forms conspicuous concretionary zones within sandstone beds. These zones are only found in the Campanian sedimentary succession and are characteristically absent in the section overlying the unconformity. All diagenetic phases encountered in the Campanian stage formed during shallow burial, and diagenetic fingerprints are well preserved as cementation reduced or prevented further alteration during later burial.

Ferroan carbonate. The Campanian sandstones are characterised by the presence of several concretionary zones of ferroan carbonate, which range from 10 cm to a few metres in thickness. These zones are difficult to identify in normal daylight but are easily recognised in UV-light. In thin section the carbonate cement stains blue, indicating a ferroan dolomite or ankeritic composition. XRD analysis indicate similar compositions. The exact composition is unknown since microprobe analysis was not applied to the cement. In the following, this cementing phase will be referred to as ferroan carbonate or ‘ankerite’.

The concretionary zones are generally pervasively cemented. They always display high primary pre-cement porosities with pointcounted values in the range of 25.5–39.5 vol-% (Tables 3–5). The sand grain configuration is generally characterised by point contacts and floating grains (Plate 3.1) indicating a very low degree of compaction prior to cementation. The same is implied by coalified wood fragments which occur undeformed or only slightly deformed with internal pore structures preserved (Plate 2.2). However, ductile grains like mudstone clasts and siderite aggregates are deformed to a certain degree to produce initial stages of pseudo-matrix. In combination, these textural relationships indicate that the sandstones experienced some, but still rather shallow burial prior to formation of ‘ankerite’ concretion zones. Compaction of uncemented sand is more advanced and is characterised by elongated and concavo-convex grain contacts with local suturing, collapse of wood fragments and highly deformed mudstone clasts and siderite aggregates (Plate 3.2). These sandstones furthermore contain sand grains with microfractures which do not occur inside the concretionary zones.

Table 3. Results of point counting of samples from Campanian channel sandstones. The point counting data were acquired to compare the amount of sandstone constituents in different samples which is the reason that volume percentages of clay phases and siderite within siderite aggregates are not corrected for microporosity. Statistical reliability with a 95 percent confidence has been calculated according to van der Plas & Tobi (1965).

Sample number	818 (vol.-%)	819 (vol.-%)	517 (vol.-%)	457 (vol.-%)	516 (vol.-%)	452 (vol.-%)	832 (vol.-%)	834 (vol.-%)	851 (vol.-%)	853 (vol.-%)	857 (vol.-%)	858 (vol.-%)	863 (vol.-%)
Detrital components													
mono-q	54.5 ± 7.0	39.5 ± 6.9	48.0 ± 7.1	42.5 ± 7.0	42.0 ± 7.0	58.0 ± 7.0	37.0 ± 6.8	53.1 ± 7.1	33.0 ± 6.6	51.5 ± 7.1	40.5 ± 6.9	34.5 ± 6.7	29.0 ± 6.4
poly-q	2.5 ± 2.2	2.5 ± 2.2	0.5 ± 1.0	2.5 ± 2.2	7.0 ± 3.6	5.0 ± 3.1	14.5 ± 5.0	10.7 ± 4.4	4.0 ± 2.8	9.0 ± 4.0	3.0 ± 2.4	4.5 ± 2.9	3.0 ± 2.4
feldspar	11.5 ± 4.5	14.5 ± 5.0	19.0 ± 5.5	7.0 ± 3.6	11.0 ± 4.4	8.5 ± 3.9	4.0 ± 2.8	11.7 ± 4.6	13.5 ± 4.8	4.0 ± 2.8	13.0 ± 4.8	11.0 ± 4.4	14.5 ± 5.0
rock fragments	0.0	0.0	0.0	0.5 ± 1.0	0.0	0.0	0.5 ± 1.0	1.0 ± 1.4	2.0 ± 2.0	0.0	0.5 ± 1.0	1.0 ± 1.4	1.0 ± 1.4
mudstone clasts	0.0	0.0	1.0 ± 1.4	0.0	2.0 ± 2.0	0.5 ± 1.0	0.5 ± 1.0	0.0	0.0	0.0	0.0	0.0	0.0
chert	0.0	0.0	0.0	0.0	0.0	0.0	0.0	0.0	1.0 ± 1.4	0.0	0.0	0.0	1.0 ± 1.4
mica	1.0 ± 1.4	1.0 ± 1.4	0.5 ± 1.0	1.0 ± 1.4	3.5 ± 2.6	0.5 ± 1.0	1.0 ± 1.4	0.5 ± 1.0	0.0	1.0 ± 1.4	1.0 ± 1.4	1.0 ± 1.4	1.5 ± 1.7
heavy minerals	0.0	0.0	0.0	0.5 ± 1.0	0.0	0.0	0.0	0.0	0.0	0.0	0.0	0.0	0.0
matrix	0.0	0.0	3.5 ± 2.6	0.0	6.5 ± 3.5	3.0 ± 2.4	1.5 ± 1.7	1.0 ± 1.4	0.0	0.0	1.0 ± 1.4	0.5 ± 1.0	0.0
plant debris	2.0 ± 2.0	7.0 ± 3.6	0.5 ± 1.0	3.5 ± 2.6	3.5 ± 2.6	0.5 ± 1.0	2.0 ± 2.0	0.5 ± 1.0	2.0 ± 2.0	2.5 ± 2.2	2.5 ± 2.2	2.5 ± 2.2	2.0 ± 2.0
Diagenetic components													
apatite	0.5 ± 1.0	0.5 ± 1.0	0.0	0.0	0.0	0.0	1.5 ± 1.7	0.0	0.0	0.0	0.0	0.0	0.0
pyrite	1.0 ± 1.4	0.0	1.0 ± 1.4	0.0	0.0	0.0	0.0	0.0	0.0	0.0	0.0	0.0	0.0
mg-siderite aggregates	1.0 ± 1.4	0.5 ± 1.0	3.5 ± 2.6	0.0	7.0 ± 3.6	2.0 ± 2.0	1.0 ± 1.4	2.6 ± 2.3	0.0	3.5 ± 2.6	10.0 ± 4.2	0.5 ± 1.0	0.0
mixed-layer clay	17.0 ± 5.3	3.0 ± 2.4	10.5 ± 4.3	6.5 ± 3.5	6.5 ± 3.5	8.0 ± 3.8	5.0 ± 3.1	9.7 ± 4.2	0.0	13.0 ± 4.8	13.5 ± 4.8	1.0 ± 1.4	2.5 ± 2.2
mixed-layer clay in feldspar	0.5 ± 1.0	0.0	0.0	0.0	0.0	0.0	0.0	0.0	0.0	0.0	0.0	0.0	0.5 ± 1.0
vermiform clay	0.0	0.0	2.5 ± 2.2	0.0	1.5 ± 1.7	0.5 ± 1.0	0.0	0.0	0.0	0.0	0.0	0.0	0.0
calcite	0.0	0.0	0.0	0.0	0.0	0.0	0.0	0.0	0.0	0.0	0.0	0.0	0.0
kaolinite	0.0	0.0	0.5 ± 1.0	0.0	0.5 ± 1.0	0.0	0.0	0.5 ± 1.0	2.0 ± 2.0	0.0	0.0	0.0	1.0 ± 1.4
kaolinite in feldspar	0.0	0.0	0.0	0.0	0.0	0.0	0.0	0.0	0.0	0.0	0.0	1.0 ± 1.4	0.0
chlorite	0.0	0.0	1.0 ± 1.4	0.0	0.0	0.0	0.0	0.0	0.0	0.0	0.0	0.0	0.0
albite	0.0	0.0	0.0	0.0	0.0	0.0	0.0	0.0	0.0	0.0	0.0	0.0	0.0
quartz	4.5 ± 2.9	1.0 ± 1.4	5.0 ± 3.1	1.0 ± 1.4	5.0 ± 3.1	5.5 ± 3.2	3.5 ± 2.6	5.6 ± 3.3	1.5 ± 1.7	12.5 ± 4.7	9.5 ± 4.1	1.5 ± 1.7	4.0 ± 2.8
ankerite/ferroan carbonate	2.5 ± 2.2	29.0 ± 6.4	0.0	33.5 ± 6.7	0.0	3.0 ± 2.4	25.5 ± 6.2	0.0	39.0 ± 6.9	0.5 ± 1.0	0.0	36.5 ± 6.8	39.5 ± 6.9
ankerite in feldspar	0.5 ± 1.0	1.5 ± 1.7	0.0	1.5 ± 1.7	0.5 ± 1.0	0.5 ± 1.0	0.5 ± 1.0	0.0	2.0 ± 2.0	0.5 ± 1.0	0.0	4.5 ± 2.9	0.0
opaque	0.0	0.0	0.0	0.0	0.0	0.0	0.0	0.0	0.0	0.0	1.0 ± 1.4	0.0	0.0
porosity	1.0 ± 1.4	0.0	2.0 ± 2.0	0.0	2.5 ± 2.2	4.5 ± 2.9	2.0 ± 2.0	3.1 ± 2.5	0.0	1.0 ± 1.4	2.0 ± 2.0	0.0	0.5 ± 1.0
porosity in feldspar	0.0	0.0	1.0 ± 1.4	0.0	1.0 ± 1.4	0.0	0.0	0.0	0.0	1.0 ± 1.4	2.5 ± 2.2	0.0	0.0
Number of counts	200	200	200	200	200	200	200	196	200	200	200	200	200

Table 4. Pointcounted samples of Campanian interchannel sandstones. Clay volume percentages are not corrected for microporosity.

Sample number	440	844	510	447	512	444	420
	(vol.-%)	(vol.-%)	(vol.-%)	(vol.-%)	(vol.-%)	(vol.-%)	(vol.-%)
Detrital components							
mono-q	50.5 ± 7.1	45.5 ± 7.0	50.5 ± 7.1	50.5 ± 7.1	54.0 ± 7.0	48.0 ± 7.1	44.5 ± 7.0
poly-q	7.0 ± 3.6	1.0 ± 1.4	16.0 ± 5.2	3.5 ± 2.6	8.5 ± 3.9	11.5 ± 4.5	4.5 ± 2.9
feldspar	4.0 ± 2.8	14.0 ± 4.9	8.0 ± 3.8	8.5 ± 3.9	5.0 ± 3.1	4.5 ± 2.9	3.5 ± 2.6
rock fragments	0.0	0.0	0.5 ± 1.0	0.0	0.5 ± 1.0	0.0	0.0
mudstone clasts	0.0	0.0	0.0	0.0	1.0 ± 1.4	0.0	0.5 ± 1.0
chert	0.0	0.0	0.0	0.0	0.0	0.0	1.0 ± 1.4
mica	1.5 ± 1.7	0.5 ± 1.0	0.5 ± 1.0	1.0 ± 1.4	2.0 ± 2.0	1.5 ± 1.7	2.5 ± 2.2
heavy minerals	0.0	0.0	0.0	0.0	0.5 ± 1.0	0.0	0.0
matrix	0.0	1.0 ± 1.4	2.0 ± 2.0	2.0 ± 2.0	5.5 ± 3.2	6.5 ± 3.5	0.5 ± 1.0
plant debris	1.0 ± 1.4	2.0 ± 2.0	1.0 ± 1.4	1.5 ± 1.7	1.5 ± 1.7	0.5 ± 1.0	8.5 ± 3.9
Diagenetic components							
apatite	0.0	0.0	0.0	0.0	0.0	0.0	0.0
pyrite	0.0	0.0	0.0	0.5 ± 1.0	0.0	0.0	0.5 ± 1.0
mg-siderite aggregates	0.0	0.0	1.5 ± 1.7	7.5 ± 3.7	2.5 ± 2.2	5.0 ± 3.1	9.5 ± 4.1
mixed-layer clay	11.0 ± 4.4	3.0 ± 2.4	4.5 ± 2.9	11.5 ± 4.5	9.0 ± 4.0	9.5 ± 4.1	13.5 ± 4.8
mixed-layer clay in feldspar	0.0	0.5 ± 1.0	0.5 ± 1.0	0.0	0.5 ± 1.0	0.0	0.0
vermiform clay	0.0	0.0	0.5 ± 1.0	0.0	0.0	0.0	0.0
calcite	0.0	0.0	0.0	0.0	0.0	0.0	0.0
kaolinite	0.0	0.0	1.0 ± 1.4	0.0	0.0	1.0 ± 1.4	0.0
kaolinite in feldspar	0.0	0.0	0.0	0.0	0.0	0.0	0.0
chlorite	0.0	0.0	0.0	0.0	0.0	0.0	0.0
albite	0.0	0.0	0.0	0.0	0.5 ± 1.0	0.0	0.5 ± 1.0
quartz	6.0 ± 3.4	1.0 ± 1.4	4.5 ± 2.9	8.0 ± 3.8	4.5 ± 2.9	9.0 ± 4.0	5.5 ± 3.2
ankerite/ferroan carbonate	10.5 ± 4.3	28.0 ± 6.3	2.5 ± 2.2	2.0 ± 2.0	0.0	0.5 ± 1.0	1.5 ± 1.7
ankerite in feldspar	0.5 ± 1.0	3.5 ± 2.6	2.0 ± 2.0	1.5 ± 1.7	1.0 ± 1.4	0.0	1.0 ± 1.4
opaque	0.5 ± 1.0	0.0	0.0	0.0	0.0	0.0	0.0
porosity	7.5 ± 3.7	0.0	3.5 ± 2.6	2.0 ± 2.0	3.5 ± 2.6	2.0 ± 2.0	2.5 ± 2.2
porosity in feldspar	0.0	0.0	1.0 ± 1.4	0.0	0.0	0.5 ± 1.0	0.0
Number of counts	200	200	200	200	200	200	200

The concretionary zones are not exclusively found along contacts to neighbouring mudstone units but most often occupy the most fine-grained part of the sandstone beds they occur in. It cannot be decided from neither the core nor from outcrop whether the concretionary zones represent lenses or laterally persistent layers.

Oxygen and carbon stable isotopes were analysed in 27 samples from two different concretionary zones (Table 6; Fig. 8). The samples were taken as 6 mm plugs.

Apatite. Apatite is observed only in the Campanian sandstones. It occurs in trace amounts as single crystals adhering to detrital grain surfaces; only in one sample (sample 832) it is porefilling, amounting to approximately 2% (Plate 4.1). The apatite has a greenish colour and always appears as 10 µm long and 5 µm wide prismatic crystals which SEM observations reveal as hexagonally outlined elongated along their c-axis (Plate 11.1). Phosphorus, calcium, and fluorine identified by EDX analysis indicate the apatite to be a fluor-apatite. Mixed-layer clay is found on apatite crystals suggesting that the clay precipitated after growth of apatite (Plate 11.2). Precipitation of thin quartz rims (described below as 1st generation quartz) post-dates apatite, which is indicated by apatite crystals often being encapsulated by quartz overgrowths.

Table 5. Pointcounted samples from Maastrichtian–Paleocene channel sandstones.
Clay volume percentages are not corrected for microporosity.

Sample number	134 (vol.-%)	865 (vol.-%)	867 (vol.-%)	869 (vol.-%)	870 (vol.-%)	873 (vol.-%)
Detrital components						
mono-q	60.5 ± 6.9	60.5 ± 7.4	65.0 ± 6.7	54.1 ± 7.4	55.4 ± 7.3	66.0 ± 6.8
poly-q	11.0 ± 4.4	14.7 ± 5.3	7.5 ± 3.7	17.1 ± 5.6	4.3 ± 3.0	8.2 ± 4.0
feldspar	2.5 ± 2.2	1.1 ± 1.6	4.5 ± 2.9	4.4 ± 3.1	6.5 ± 3.6	4.6 ± 3.0
rock fragments	1.5 ± 1.7	1.7 ± 1.9	0.0	1.1 ± 1.6	0.5 ± 1.1	0.5 ± 1.0
mudstone clasts	2.0 ± 2.0	0.6 ± 1.1	0.0	0.6 ± 1.1	1.1 ± 1.5	0.5 ± 1.0
chert	0.0	0.0	0.0	0.0	0.0	0.0
mica	1.0 ± 1.4	0.0	0.0	0.0	0.0	0.0
heavy minerals	0.0	0.0	0.0	0.0	0.0	0.0
matrix	0.0	1.1 ± 1.6	0.5 ± 1.0	2.2 ± 2.2	6.5 ± 3.6	5.7 ± 3.3
plant debris	0.0	0.0	0.0	0.0	0.0	0.0
Diagenetic components						
apatite	0.0					
pyrite	0.0	0.0	0.0	0.0	0.0	0.0
mg-siderite aggregates	0.0	0.6 ± 1.1	0.0	1.7 ± 1.9	0.0	0.0
mixed-layer clay	3.0 ± 2.4	< 1	< 1	< 1	< 1	< 1
mixed-layer clay in feldspar	0.5 ± 1.0	0.0	0.0	0.0	0.0	0.0
vermiform clay	0.0	0.0	0.0	0.0	0.0	0.0
calcite	0.0	0.0	0.0	0.0	0.0	0.0
kaolinite	0.0	0.0	0.5 ± 1.0	0.0	0.5 ± 1.1	0.5 ± 1.0
kaolinite in feldspar	0.0	0.0	0.0	0.0	0.0	0.0
chlorite	0.0	0.0	0.0	0.0	0.0	0.0
albite	0.0					
quartz	6.5 ± 3.5	0.0	2.0 ± 2.0	1.7 ± 1.9	1.1 ± 1.5	0.5 ± 1.0
ankerite	3.0 ± 2.4	1.7 ± 1.9	0.5 ± 1.0	0.6 ± 1.1	0.5 ± 1.1	1.0 ± 1.5
ankerite in feldspar	1.0 ± 1.4	0.0	0.0	0.0	0.0	0.0
opaque	0.0	0.0	0.0	0.6 ± 1.1	1.1 ± 1.5	1.5 ± 1.8
porosity	7.0 ± 3.6	18.1 ± 5.8	19.5 ± 5.6	16.0 ± 5.5	22.3 ± 6.1	10.8 ± 4.5
porosity in feldspar	0.5 ± 1.0					
Number of counts	200	177	200	181	184	194

Pyrite framboids. Pyrite as framboids are observed in trace amount in all samples where they attain sizes up to 10–15 µm. The framboids occur within mixed-layer clay rims (Plate 11.2), or may be overgrown by 1st generation quartz within the concretionary zones. A reliable relative timing between framboid formation and apatite growth was not established.

Siderite. Three textural types of Mg-siderite are recognised: (1) microcrystalline crystals arranged in aggregates, (2) microcrystalline crystals associated with detrital micas, and (3) fine- to medium-crystalline crystals primarily associated with feldspar. All types are observed in the Campanian as well as in the overlying sandstone beds but Mg-siderite type 3, which has not been encountered within the concretionary zones, is believed to have formed much later during the Maastrichtian–Paleocene diagenetic stage.

Table 6. Oxygen and carbon stable isotopes of samples from two concretionary zones.

Isotope sample number	δO^{18} PDB	δC^{13} PDB	Distance below top of zone (mm)
1	-7.05	-12.27	2042
2	-7.19	-7.84	1842
3	-6.05	0.69	1708
4	-7.9	1.5	1583
5	-6.23	2.96	1458
6	-8.56	0.07	963
7	-6.39	2.62	638
8	-6.36	-0.53	396
9	-7.44	-9.21	204
10	-7.36	-14.55	140
11	-6.84	-10.57	75
12	-8.05	-9.12	50
13	-6.89	-11.51	698
14	-7.39	-10.1	642
15	-7.14	-8.62	550
16	-5.61	2.15	479
17	-6.38	1.96	442
18	-6.4	1.58	396
19	-6.04	0.16	327
20	-6.13	-0.58	288
21	-6.11	-1.06	258
22	-6.54	-1.96	217
23	-6.64	-2.62	183
24	-7.09	-8.84	133
25	-6.86	-11.45	88
26	-7.21	-7.67	42
27	-8.66	-7.67	8

Sample no. 01–12:2.05 m thick zone, top of zone at 763.9 m depth (Box 233B–232C).

Sample no. 13–27:0.71 m thick zone, top of zone at 741.5 m depth (Box 225C).

Mg-siderite type 1 (siderite aggregates) constitutes less than 10% by volume in pointcounted samples (Tables 3–5), but may reach up to 25–40% by volume in other samples. The aggregates have a reddish-brown colour when observed in thin section (Plate 4.2), and individual crystals never exceed 10 μm (Plate 13.5, 13.6). The size of the aggregates equals that of the framework detritals and the shape and relations to adjacent detrital grains show deformation structures similar to those developed by the mudstone fragments (Plates 4.2, 13.5). The aggregates are thus interpreted as compactionally deformed. Back-scatter imaging combined with microprobe analysis performed on 10 samples revealed that the aggregates consist of euhedral to subhedral crystals set in an Al-silicate matrix (Plates 13.1–7) which partly consists of flaky clay crystals smaller than 3 μm (Plate 13.2). It thus seems likely that the Mg-siderite precipitated within a clay matrix.

Type 2 Mg-siderite form 2–10 μm large, euhedral to subhedral crystals aligned along cleavage planes within muscovite and biotite (Plate 13.8). The siderite crystals occur most abundantly in biotite grains indicating that its growth was controlled by supply of Fe^{2+} liberated by decomposition of the biotites and muscovites. The siderite aggregates (type 1 siderite) could represent almost totally re-

placed biotite but that is probably not the case since only a slight replacement and not a full range of replacement is observed elsewhere.

Microprobe analysis was carried out on all three identified types of siderite. A total of 45 crystals were analysed; 20 analyses were carried out on types 1 and 3 respectively and 5 analyses on type 2. The mole-percentage of MgCO_3 , FeCO_3 and CaCO_3 for all analyses are given in Figure 5. Concerning contents of magnesium and iron all types display similar compositions, varying between 20 and 54 mole-% MgCO_3 (Fig. 6). However, types 1 and 2 (microcrystalline types) differ from type 3 (fine- to medium-crystalline type) by a somewhat higher content (about 2–3 mole-%) of CaCO_3 (Fig. 5). Three standardless measurements using EDX equipment on a scanning electron microscope are listed in Table 7. These were obtained in conjunction with back-scatter imaging (Plate 13.1–8) and are in good agreement with the microprobe analyses.

Growth relations between the three siderite types and any other cementing phase are all in all unknown. However, the occurrence of types 1 and 2 within concretionary zones demonstrates these phases to have been active prior to the ferroan carbonate cementing event.

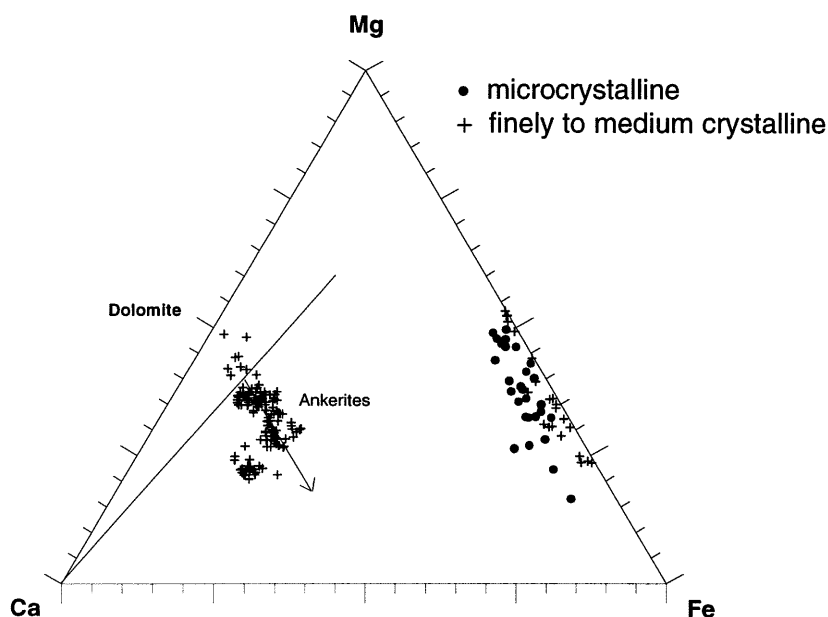


Figure 5. Carbonate composition in mole-% calcite-magnesite-siderite.

First generation quartz. Early quartz forms thin, euhedral overgrowths on quartz grains embedded within the concretionary zones. The overgrowths are partial and generally less than 20 μm in thickness. The amount of overgrowth varies from sample to sample from nearly absent to pointcounted 4 vol-%. Fluid inclusions are observed at the base of 1st generation quartz overgrowths. These overgrowths are easily recognised when embedded

within the 'ankerite' cement. They are, however, difficult to discriminate from later quartz generations outside the concretionary zones without the application of more sophisticated methods like hot-cathode luminescence. First generation quartz encompasses earlier formed apatite crystals and pyrite framboids.

Table 7. Standardless analysis, livetime: 60,0 sec; Acc. volt.: 15kV

	1		2		3		4	
	Atom%	Element wt-%	Atom%	Element wt-%	Atom%	Element wt-%	Atom%	Element wt-%
Si-K	1,77	1,19	0,46	0,28	53,02	51,50	1,47	0,88
Al-K	1,11	0,72	0,00	0,00	36,81	34,35	0,48	0,27
Ca-K	5,33	5,10	0,74	0,63	0,40	0,56	0,44	0,38
Mg-K	38,47	22,33	26,31	13,58	0,43	0,36	24,78	12,81
Na-K	0,43	0,24	0,69	0,34	0,26	0,21	1,03	0,50
K-K	0,25	0,24	0,00	0,00	7,78	10,52	0,42	0,35
Fe-K	52,63	70,19	71,79	85,17	1,30	2,51	71,39	84,81
Total	100,00	100,00	100,00	100,00	100,00	100,00	100,00	100,00

1. Microcrystalline Mg-siderite; 2. Finely crystalline Mg-siderite; 3. Al-Si-matrix; 4. Finely crystalline Mg-siderite.

Mixed-layer clay. Clay interpreted as mixed-layer clay occurs in all samples. Within the concretionary zones the clay forms porelinings up to 5 μm in thickness on detrital grains, with individual clay flakes tangentially oriented. The interference colours of the clay are up to 2nd order yellow and thus indicate a high birefringence which is in agreement with a mixed-layer illite/smectite or illite/vermiculite clay composition. Clay with similar texture occurs outside the concretionary zones where XRD analysis of one sample determined the clay as mixed-layer illite/vermiculite. SEM analysis display crinkly clay flakes with thin and very short spiny projections.

Pointcounting indicates that the mixed-layer clay within the concretionary zones may constitute up to 7% of the rock volume (Table 3). However, SEM observations indicate that the clay is highly microporous so that the actual amount of clay probably gets no larger than about 2%.

Mixed-layer clay rims cover 1st generation quartz overgrowths thereby postdating it.

Feldspar dissolution and kaolinite precipitation. Kaolinite is found as small aggregates of booklets infilling feldspars but never in primary pores (Plate 5.2). Outside the concretionary zones kaolinite is likewise found in secondary pores within feldspar but also in oversize pores not accompanied with feldspar.

Post-Campanian diagenetic stage

Early alterations recognised in the Maastrichtian–Paleocene succession are characterised by initial precipitation of pyrite framboids and siderite followed by precipitation of quartz overgrowths, mixed-layer clay rims and probably also by pore-cementing calcite. Contemporaneous with these alterations, the porelining mixed-layer clay in the underlying Campanian succession is believed to have developed further.

Later alterations affecting the total package of Paleocene and Cretaceous sandstones penetrated by the well are characterised by dissolution of feldspar followed by precipitation of kaolinite, albite, quartz, siderite and finally ankerite.

Early diagenetic events

Pyrite framboids. Pyrite forms up to 15 µm large, single framboids adhering to detrital grain surfaces, or as single crystals and aggregations within porous wood fragments.

Siderite. Mg-siderite types 1 and 2 which are described above also occur in the Maastrichtian–Paleocene part of the succession penetrated by the GANT#1 well.

Second generation quartz. Second generation quartz forming early overgrowths in the Maastrichtian–Paleocene succession are very similar to the early quartz overgrowths observed in the Campanian succession, and post-date pyrite framboids.

Mixed-layer clay. Mixed-layer clay commonly forms thin porelinings in the Maastrichtian–Paleocene sandstones. The clay amounts to less than 1 vol.-% (pointcounted) and covers the 2nd generation quartz overgrowths (Plates 11.3, 13.4). Secondary porosity within rimmed detrital feldspars never contains internal filling of mixed-layer clay thus indicating that the clay precipitated prior to dissolution of feldspar (Plate 6.1).

A single sample shows more extensive development of the mixed-layer clay phase (pointcounted 3.0 vol.-% without correction for microporosity). This sample has anomalously thick (up to 20 µm) grain coatings and common fillings of fractures in feldspar grains (Plates 11.5, 13.6). Furthermore,

dissolution cavities in feldspars occurring next to the fracture fillings do not contain mixed-layer clay (Plate 11.6). The individual flakes of the coatings are oriented perpendicular to the overgrown grains and the coatings are postdated by 3rd generation quartz (Plate 11.7). This sample was taken only 20 cm from a 55 cm thick intrusion and probably owes the anomalous clay development to the presence of this sill.

In the Campanian succession, porelining clay appears to be more voluminous in the uncemented sandstones (pointcounted 6.5–17 vol.-%) than within concretionary zones (pointcounted <7 vol.-%) (Tables 3–5). In addition it occurs as rare fillings in fractured sand grains and locally attain a porefilling appearance. This difference is interpreted as caused either by continued or by renewed clay growth following precipitation of the ferroan carbonate cement.

One sample from the Maastrichtian–Paleocene succession was selected for XRD analysis to determine the nature of the mixed-layer clay. The analysis indicates an illite/vermiculite clay very similar to the clay analysed from Campanian sandstone. When viewed in SEM the clay crystals are seen to form crinkly flakes with spiny projections. Such morphology has been described as indicating mixed-layer I/S clay (Wilson & Pittman 1977). All reported occurrences of illitic clays indicate that spiny projections are a feature related to the illite clay component. The interference colours of the clay are up to 2nd order yellow and thus indicate a high birefringence in agreement with this composition.

Calcite. Calcite is very rare and only observed in sandstones overlying the unconformity. The calcite forms scattered porefilling of primary pores, totally cementing one to three adjacent pores, and is also observed to have crystallised inside dissolution caves in feldspar grains. Upon staining, the calcite crystals display zonation, being iron-poor in the centres (red staining) and more iron-rich (bluish or mauve staining) along their margins (Plate 6.2).

The limited occurrence of the calcite did not allow establishment of the relative timing of growth to other phases in any greater detail. However, calcite is observed to overlie thin quartz overgrowths, thus postdating 2nd generation quartz overgrowths. The growth relation to mixed-layer clay is not established, but precipitation of the mixed-layer clay and the calcite is considered to be the latest of the early diagenetic events.

A single sandstone sample from 166.0 m depth was powdered, the calcite part dissolved and oxygen and carbon isotope values determined. The isotopic composition is $\delta^{18}\text{O} = -11.04\text{‰}$ PDB and $\delta^{13}\text{C} = -2.90\text{‰}$ PDB.

Late diagenetic events

Late alterations affect both Maastrichtian–Paleocene sandstones and the Campanian sandstones which are not cemented by ferroan carbonate. These late diagenetic changes dominantly took place in detrital intragrain positions since most of all primary porosity was obliterated by compaction and other preceding diagenetic alterations.

Feldspar dissolution. All samples contain a range of unaltered to partly dissolved detrital feldspar grains as well as isolated, oversized pores. The latter are assumed to result from complete dissolution of feldspar grains, but may also develop from complete dissolution of other labile detrital grains.

Feldspar dissolution is clearly predated by the mixed-layer clay rims and is postdated by quartz overgrowths which invade and partly fill dissolution cavities (Plate 6.1). Most of the compaction is interpreted to have occurred prior to feldspar dissolution since only a few skeletal dissolution remnants are observed to have collapsed (Plates 6.1, 7.1).

Kaolinite. Kaolinite occurs as two textural types: (1) as porefilling aggregates of booklets and (2) as a vermiform replacement product of biotites and within mudstone clasts.

Aggregates of kaolinite booklets are present in all samples but constitute less than 2 vol.-% (Tables 3–5). Individual platelets in the booklets have diameters of *c.* 20 μm and are less than 1 μm thick. The aggregates may fill secondary pores in feldspars partly or totally, or they may occur as aggregates not associated with feldspars. However, these latter aggregates have sizes and shapes resembling that of detrital grains (Plate 8.1) which suggest that they represent total replacements after feldspar. The kaolinite precipitation is postdated by some grain dissolution since it occurs next to empty secondary pores without entering these (Plate 8.1). It is thus likely that more or less contemporaneous dissolution of feldspar and precipitation of kaolinite occurred. Kaolinite booklets are also found encapsulated within 3rd generation quartz overgrowths which clearly formed after dissolution of feldspars (Plate 12.1)

Vermicular kaolinite occurs as replacement products in up to 150 μm stackings within biotites and mudstone clasts, but are in both cases very rare.

Albite. Authigenic albite occurs as syntaxial, minute crystals on corroded surfaces of detrital feldspar grains (Plate 11.8) or on feldspar remnants within skeletal grains (Plates 7.1, 7.2) indicating that it post-dates feldspar dissolution. Individual albite crystals are always smaller than 40 μm and, although authigenic albite is common, it amounts to less than 1 % of the bulk volume.

Chlorite. Chlorite is observed in three samples only (134, 517, 459), and never exceeds 1 vol.-% (Table 3). Identification is based on thin section, SEM and XRD. Chlorite occurs both as fans (Plate 8.2) and rosettes, with rosettes recognised only in sample 134 (Plate 12.2).

Chlorite as fans has a greenish colour in thin section. SEM observations show the fans to consist of irregularly shaped hexagonal flakes with diameters persistently around 25 μm . The chlorite often occurs in the vicinity of detrital feldspars, but apparently never infills skeletal feldspars. The fans were frequently encountered next to authigenic albite crystals, but not in a manner which reveals any growth relationship (Plate 11.8).

Chlorite occurs captured within 3rd generation quartz overgrowths, thus predating this quartz phase (Plate 8.2).

All samples containing chlorite occur in the near vicinity of dolerite intrusions. This suggests that the presence of sills may have controlled chlorite stabilisation.

Third generation quartz. These overgrowths differ from the earlier 1st and 2nd generation by thickness and textural position. Where 1st and 2nd generation overgrowths are thin and restricted to primary porosity, 3rd generation overgrowths are outgrowth-like and characteristically developed as short and stubby crystals which are often found projecting into empty moulds (Plate 9.1) or into partly

dissolved detrital feldspars. They are also considerably thicker than 1st and 2nd generation overgrowths, generally 60–100 μm (Plates 9.1, 9.2).

Third generation quartz may owe its stubby growth to the common presence of mixed-layer clay coatings, which left only restricted patches of free surface on the detrital quartz grains to act as nucleation sites. Commonly, the overgrowths also overlie the coatings (Plate 9.2) and may encapsulate kaolinite booklets.

First, second and third generation overgrowth bases are often lined by inclusions of minute mineral phases which, however, are not possible to identify properly with the optical microscope.

Type 3 Mg-siderite. Late type 3 Mg-siderite forms crystals 20–100 μm in size, which generally occur intergrown with ankerite. However, both siderite and ankerite have similar stain-colours which makes differentiation in thin section difficult and tedious. Mg-siderite can be observed easily on back-scatter images of polished thin sections with SEM or microprobe, and textural observations are mostly obtained by these methods but only a limited number of observations were obtained. However, in all cases the siderite was observed to be associated with detrital feldspar grains mostly occurring within secondary dissolution porosity (Plate 13.4). Type 3 Mg-siderite is difficult to recognise in thin sections; however, it seems to occur in trace amounts only. Further investigations are necessary to get some convincing textural relationships in order to fit the formation of this siderite into a paragenetic sequence. Mg-siderite from other settings are reported to occur late in the diagenetic sequence prior to ankerite formation (e.g. MacAulay *et al.* 1993).

Ankerite. All investigated samples of Maastrichtian–Paleocene sandstones as well as uncemented Campanian sandstones contain a minor, but significant amount of ankerite cement (less than 3 vol.-%; Table 3). This ankerite is very often found within dissolution cavities in detrital feldspar grains and within oversize pores which are partly or sometimes totally infilled. The porefill consists of one to five ankerite crystals varying in size from 30 μm to the size of the infilled pores and individual crystals have euhedral outlines when not filling pores completely. It post-dates the main phase of 3rd generation quartz overgrowth by further reducing porosity. Although the outlines of the ankerite crystals are intact, they are slightly corroded (Plate 12.3).

Results from microprobe analyses of the ankerite define an elongated compositional field from ferrodolomite to ankerite (Fig. 5). The iron content varies between 5 and 25 mole-% FeCO_3 , and most of the point compositions classify as ankerite (Deer *et al.* 1992).

Concretionary pyrite. Pyrite concretions are 1–2 cm in diameter. They are unevenly distributed in the core but quantification of this phase has not been carried out; however, several concretions are present in the interval between 742 m and 758 m.

The pyrite concretions are characterised by a greenish tint and by marginal reddish-brown haloes. The concretions seem to consist of cubes 5–50 μm in size (Plate 12.4) which also may occur thinly distributed in the vicinity of the concretions. Third generation quartz overgrowths and ankerite cement occur within the concretions, and microfractures in detrital grains within the pyrite concretions are filled with pyrite all indicating that the pyrite concretions formed very late (Plate 10.1) but the actual control on their formation is still unclear.

Microfractures

Microfracturing of all types of rigid detrital grains occur. They are most common in feldspar, whereas lesser amounts of quartz grains are fractured. Among the quartz grains particularly the polycrystalline grains are fractured, with the microfractures developed between individual crystals. In the Maastrichtian–Paleocene sandstones fracturing of quartz is markedly less developed than in the Campanian sandstones. A few microfractures are observed filled with ankerite and/or quartz cement (Plate 10.2). This infilling quartz cement is observed in optical continuity with 3rd generation quartz cement found on the outer grain surface and is therefore interpreted as also belonging to the 3rd generation phase.

The characteristic microfracturing of the rigid detrital grains together with the poorly developed pressure solution features (sutured grain contacts are rarely observed) may suggest rapid burial.

Mudstones

Preliminary XRD study on 22 GANT#1 mudstone samples spanning the full core interval indicated a mudstone clay mineral assemblage consisting of smectitic clay, illite and kaolinite. This assemblage showed a downwards change from an assemblage within the $<2 \mu\text{m}$ size fraction dominated by smectitic clay to an assemblage dominated by kaolinite together with some mixed-layer clay (Kierkegaard 1997).

In order to examine the character of the smectitic and mixed-layer clay in more detail, four mudstone samples were selected and analysed in the size fractions $<0.2\mu\text{m}$ and $0.2\text{--}2 \mu\text{m}$ (Table 8).

All samples show an appreciable content of kaolinite. The two uppermost samples have strong maxima in the 10 to 17 Å region representing well-defined, random layered, highly smectitic illite/smectite mixed-layer clay (Fig. 6a, b). In both of these samples this mixed-layer clay has only a minor content of illite interlayers, the sample at 65 m having little more illite than the sample at 268 m. According to smectite behaviour, saturation with KCl causes the maxima to collapse to 11.7–12.1 Å. However, heating to 300°C failed to collapse these maxima much further, causing collapse to 11.2–12.1 Å only. This suggests that the mixed-layer structure might contain interlayers of chlorite or of organic molecules prohibiting further collapse upon heating. Organic molecules as a possibility has to be taken into account, because the samples were not treated with oxidising agents to remove organic matter. The $0.2\text{--}2 \mu\text{m}$ size fractions display small and sharp 10 Å peaks which probably represent not only the signal from the illite component in the mixed-layer clay phase, but also discrete illite and/or mica.

The samples from 400 m and 875 m both contain a composite maxima in the 10–15 Å region consisting of a broad maximum around 13 to 15 Å and a well defined peak at 14.3 Å (Fig. 6a, b). Neither glycolation nor glycerolation caused swelling, while saturation with KCl caused collapse of both peaks. The maxima are taken to represent mixed-layer illite/vermiculite and discrete vermiculite, respectively. KCl saturation and heating to 300°C both caused collapse to $c.11 \text{ Å}$ only, implying possible interlayers of chlorite or organic molecules within the mixed-layer structure, similar to the two uppermost samples. Sharp 10 Å peaks are present in the $0.2\text{--}2 \mu\text{m}$ size fractions implying presence of discrete illite and/or mica also similar to the two uppermost samples.

It is not known whether the transition from illite/smectite to illite/vermiculite is gradual or sharp but a sharp transition implies a shift in provenance.

Table 8. Clay mineral assemblages of mudstones.

Depth (m)	Sample no.	Clay mineral assemblage		
65	879	I/S, smectite dominated	Kaolinite	
268	878	I/S, smectite dominated	Kaolinite	
400	877	I/V, vermiculite dominated	Kaolinite	Discrete vermiculite
875	876	I/V, vermiculite dominated	Kaolinite	Discrete vermiculite

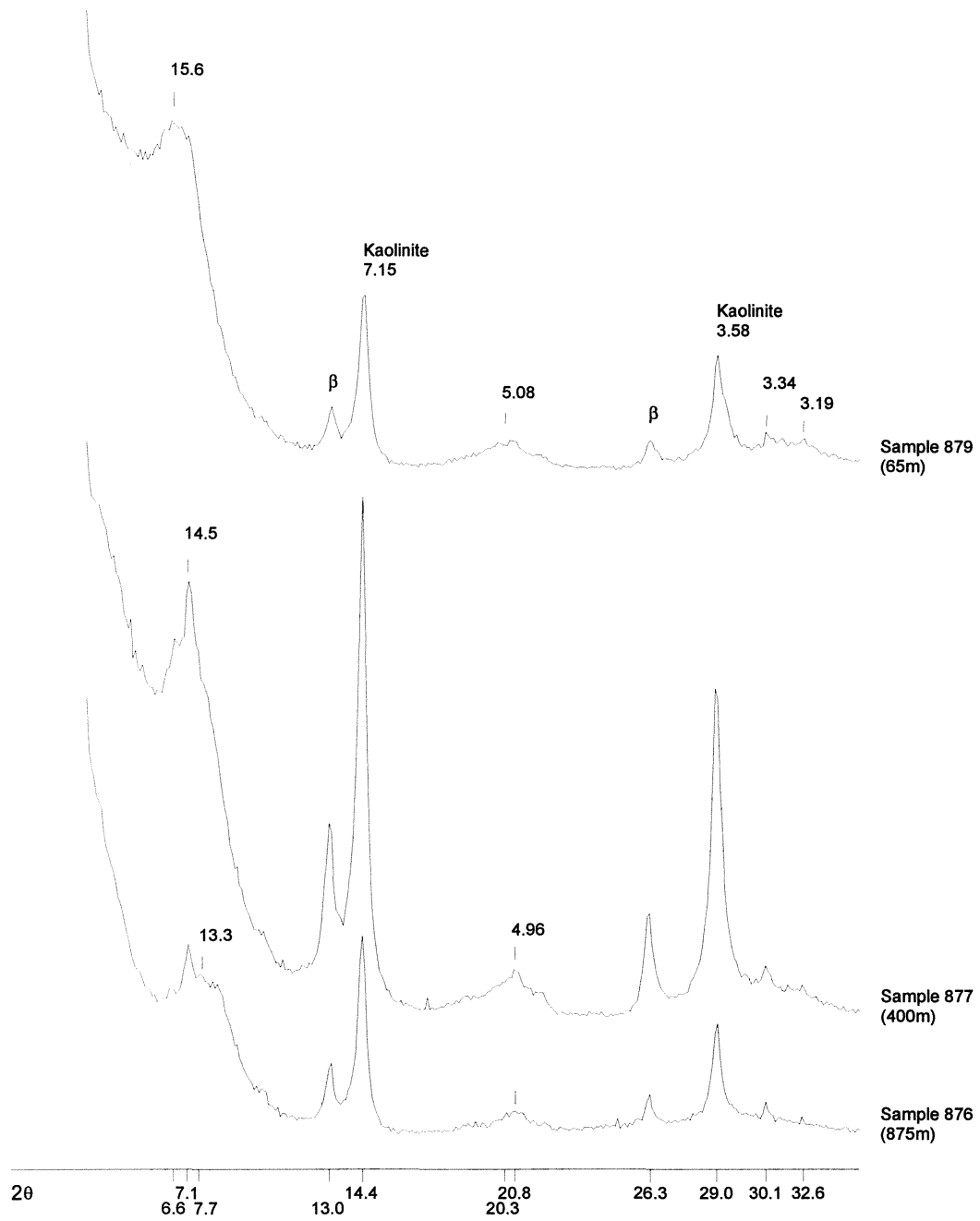


Figure 6a. Clay mineralogy of mudstones, <math><0.2\ \mu\text{m}</math> size fraction. Mg-saturated (Cobalt radiation).

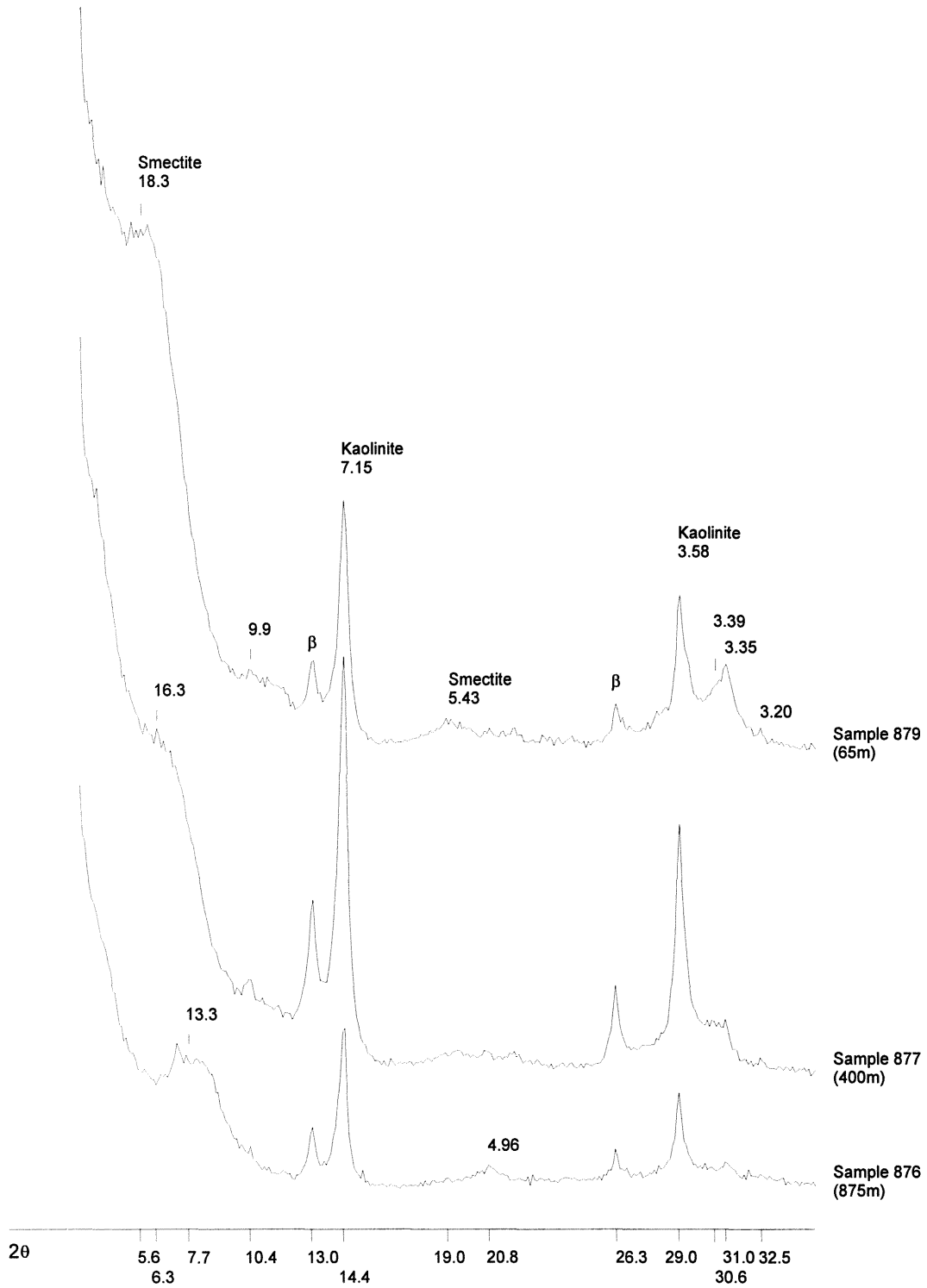


Figure 6b. Clay mineralogy of mudstones, <math><0.2\ \mu\text{m}</math> size fraction. Ethylene-glycolated Mg-saturated samples (Cobalt radiation).

Intrusion-related diagenetic effects

The diagenesis in the GANT#1 well was not studied specifically in order to explore the influence of intrusions. However, chlorite was observed only in the near vicinity of intrusions (Fig. 2, samples 134, 517 and 459) and abnormally high amounts of mixed-layer clay were observed in two samples close to sills (Fig. 2 samples 818 and 134). These observations from the GANT#1 well are in line with observations by Esposito & Whitney (1995), and it is believed that at least chlorite growth was controlled by the presence of the sills. Whether the chlorite growth is a syn- or post-emplacement phase is not known. The chlorite and mixed layer clay mentioned above predate 3rd generation quartz.

Diagenetic model

A general model for the diagenetic changes seen in the GANT#1 core involves shallow burial diagenesis of the Campanian sediments comprising growth of apatite, pyrite, siderite, quartz and mixed-layer clay. This was succeeded by a relative sea-level fall probably giving access for meteoric dominated pore water and formation of ferroan carbonate concretionary zones (Fig. 7). Following renewed deposition, burial diagenesis, including continued compaction, affected the total package of sediments. The formation of early pyrite, siderite and 2nd generation quartz was not revived within the Campanian succession because conditions leading to these processes did not exist any more. Calcite only occurs within the Maastrichtian–Paleocene succession. All other events, i.e. mixed-layer clay, dissolution of feldspars, precipitation of kaolinite, albite, 3rd generation quartz, type-3 siderite and late ankerite influenced the total package during the post-Campanian diagenetic stage (Fig. 7).

		Campanian burial	Post-Campanian burial
Shallow burial	Apatite	—	
	Pyrite framboids	—	—
	Siderite type 1	—	—
	Early quartz	—	—
	Mixed-layer clay	—	— ? —
	Ferroan carbonate	—	
	Calcite		—
Deep burial	Feldspar dissolution		—
	Kaolinite		—
	Albite		—
	Third generation quartz		—
	Siderite type 3		?
	Ankerite		—
	Pyrite concretions		—
	Compaction		—

Figure 7. Paragenetic sequence of diagenetic events during the Cretaceous and Paleocene.

Campanian diagenetic stage

The Campanian sandstones are deposited in a marine fault-controlled slope environment (Dam 1996), and both the mineral assemblage within the concretionary zones and its sequential order are in concord with progressive burial in a marine, eogenetic environment (i.e. precipitation from evolved marine porewaters) (Burley *et al.* 1985). The relative timing of apatite and the pyrite framboids is not established but studies of carbonate-flourapatite nodules in muds of the Peru–Chile outer shelf and upper slope suggest that the phosphate mineral precipitated before the sulfidic pyrite (Glenn & Arthur 1988). Pyrite precipitates in the sulfate reduction zone during early diagenesis when marine sulfate is still available together with reduced iron (Berner 1984). Siderite type 2 is more abundant in biotite

than in muscovite indicating that the iron in the siderite was supplied by the micas. This suggests that local geochemical environments with raised pH near degrading micas favoured the precipitation of carbonates (Boles & Johnson 1984). The aggregates forming siderite type 1 are much more problematic since they could have formed within the sandstones (maybe in a similar way as siderite type 2) or in the uppermost parts of the interchannel mudstones following sulfide reduction (Gautier *et al.* 1985). Mozley (1989) documented that marine siderite is extremely impure with up to 41 mole-% $MgCO_3$ and 15 mole-% $CaCO_3$, whereas freshwater siderite contains more than 90 mole-% $FeCO_3$. The chemical composition of the GANT#1 type-1 and type-2 siderite is comparable to the compositional range of marine siderites. Samples from Maastrichtian–Paleocene sandstones often contain both siderite aggregates and mudstone clasts. However, the mudstone clasts do not contain siderite implying that the siderite did not precipitate within the sandstones. It is thus likely that the siderite aggregates represent intraformational interchannel mudstone clasts which are not a part of the detritus sourced from the hinterland. Quartz cementation is postdated by the formation of clay rims which probably is the latest phase to form before cementation with ferroan carbonate.

The low degree of compaction of the sand within the concretionary zones could suggest that cementation with ferroan carbonate occurred very early after deposition, but the presence of the earlier mineral phases indicates that ferroan carbonate cementation was the final stage of a succession of prograding marine diagenetic events.

Oxygen and carbonate isotope analyses sampled across two concretionary zones demonstrate a

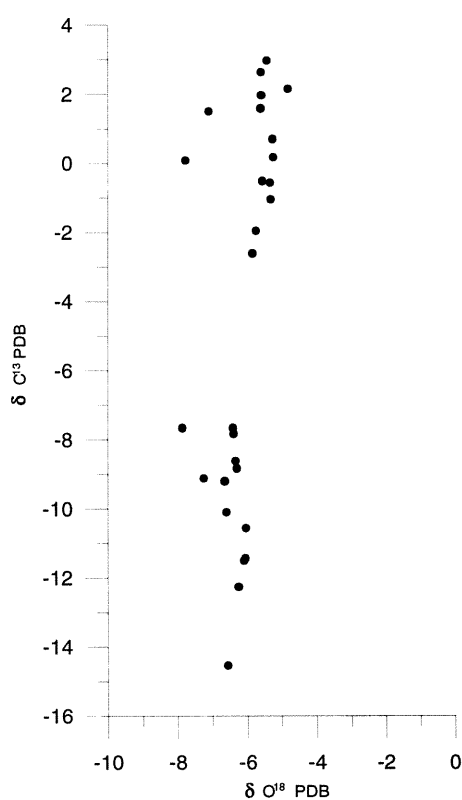


Figure 8. Cross-plot of δO^{18} and δC^{13} compositions of ferroan carbonate from two concretionary zones.

broad $\delta^{13}C$ variance from -14,55 to +2,96‰ PDB and a relatively narrow $\delta^{18}O$ variance from -8,66 to -5,61‰ PDB (Fig. 8). The zones which are considered to represent single concretions, show a trend from positive $\delta^{13}C$ -values at the centre of the zones to negative $\delta^{13}C$ -values at the margins, but oxygen isotope values do not show a well defined trend (Table 6). The carbon isotope trend can be interpreted as resulting from mixing of two bicarbonate sources characterised with heavy and light carbon isotope compositions (Kantorowicz 1985) but is not studied in further detail. The $\delta^{18}O$ -values of the ferroan carbonate show that the porewater it precipitated from is more negative than the $\delta^{18}O$ -value of Late Cretaceous sea water which is considered to be between -2 and 0‰ SMOW (Mozley & Burns 1993). Using the isotope fractionation equation $1000\ln\alpha = 2.78 \times 10^6 T^{-2} + 0.11$ (Fisher & Land 1986) the ferroan carbonate is found to have precipitated from waters with a range in isotopic composition from -3.99 to -1.19‰ $\delta^{18}O$ SMOW or from -10.29 to -7.04‰ $\delta^{18}O$ SMOW at 50 and 20°C, respectively. Both mixing and sediment-water interaction can change the $\delta^{18}O$ -value of seawater but the small rock-water ratio prior to carbonate cementation suggests mixing to be the most likely process. Meteoric water would probably both lower the $\delta^{18}O$ -values of the porewater and act as a large

reservoir resulting in the observed small variation in oxygen isotope composition (Fig. 8). A broad variation of $\delta^{13}\text{C}$ -values together with a small variation of $\delta^{18}\text{O}$ -values is proposed to indicate a meteoric influence of subsurface limestones (Allan & Matthews 1977). The same trend in isotope compositions is also reported from ankerites precipitated during shallow burial in sandstones (Dutton & Land 1985; Longstaffe & Ayalon 1987).

The key to unravel the diagenetic history of the GANT#1 well is thus the ferroan carbonate concretionary zones which are related to the formation of the major erosional unconformity recognised at 255.85 m in the well separating Campanian sediments from the overlying Maastrichtian–Paleocene succession (Fig. 2). This conclusion is supported by:

- 1) that the concretionary zones only occur in Campanian sandstone beds, and
- 2) that they have formed under the influence of meteoric water, as suggested by oxygen and carbon stable isotopes, succeeding shallow burial formation of apatite, pyrite, siderite, thin quartz overgrowths and mixed-layer clay, which are all considered as phases developed in sediments influenced by evolved marine pore waters.

The high minus-cement porosity (25,5–39,5%) indicates a low degree of compaction and shallow depth of burial. The actual maximum depth of burial of the Campanian sediments before cementation with ferroan carbonate and relative sea level drop is unknown. Feldspar leaching and kaolinite precipitation within sandstones are reported to occur in meteoric influenced environments even when carbonate is present in the sediment (Bjørlykke & Aagaard 1992) or at deeper burial when acids are released by maturation of organic matter in adjacent shales (Ehrenberg 1991). However, the low degree of compaction observed in the concretionary zones seems to preclude deep Campanian burial. The kaolinite present within feldspars in the concretionary zones may thus be related to meteoric influence during the Maastrichtian relative sea level fall or to organic maturation during deeper Paleocene burial.

Post-Campanian diagenetic stage

Pyrite framboids, siderite aggregates (siderite type 1), 2nd generation quartz overgrowths and mixed-layer clay pore linings are all present in the Maastrichtian–Paleocene succession. These phases occur in a similar way and order as observed in the Campanian diagenetic stage indicating that the same shallow burial diagenetic processes were active. The remaining diagenetic alterations all occurred later than the main phase of compaction, and they all influenced the total succession of penetrated Cretaceous and Paleocene strata.

The delicate structure of skeletal feldspar grains developed by dissolution which has remained intact indicate that sandstones had stabilised mechanically prior to the dissolution event. Kaolinite precipitation in GANT#1 is intimately connected with feldspar dissolution and is controlled by either surface or deeper burial processes. Feldspar dissolution and kaolinite precipitation during burial commonly occur at temperatures able to generate organic acids or CO_2 from thermal decarboxylation processes in shales (Surdam *et al.* 1989; Ehrenberg 1991). The content of total organic carbon (TOC) in the mudstones of the GANT#1 core is moderate to high with most values between 2.5% and 8% (Christiansen *et al.* 1996). In general, most sandstone diagenetic phases occurring during burial

of a sandstone-mudstone dominated succession are a result of interaction between processes occurring in the mudstones and the interbedded sandstones (Boles & Franks 1979; Burley *et al.* 1985).

The downwards shift from highly smectitic mixed-layer illite/smectite clay to mixed-layer illite/vermiculite clay in the GANT#1 core may represent either a change in sediment provenance or a diagenetic transition. Organic maturity data from the GANT#1 well indicate a shift from thermally immature to mature around 350 m (Christiansen *et al.* 1996) which coincides with the change from illite/smectite to illite/vermiculite occurring in the mudstones in the interval between 270 and 400 m. This suggests that the change in mudstone composition probably is related to burial diagenesis – a conclusion which is in concord with diagenetic alterations observed in the sandstones.

Decomposition of smectite to illite releases silica, sodium, calcium, iron and magnesium in varying quantities dependent on the original composition of the smectitic clays. Silica released from a smectite to illite transition may form quartz overgrowth, sodium may be involved in albitisation processes and magnesium and iron may form chlorites from kaolinite and ankerite from calcite (Burley *et al.* 1985). In GANT#1 quartz overgrowth, albite crystals and ankerite cement is present (Table 9).

Campanian sandstones contain more quartz cement and mixed layer clay than post-Campanian sandstones (Table 9). A similar difference in late ankerite cementation of the two intervals is evident from visual inspection of the thin section although it is not revealed by point counting (Table 9). This change in cementation of sandstones parallels the change from illite/smectite to illite/vermiculite in mudstones since all Campanian sandstones occur below the illite/vermiculite level at 400 m whereas the Maastrichtian–Paleocene sandstones occur above the illite/smectite level at 270 m.

Table 9. Volume percentages measured by pointcounting of the most important cementing phases and porosity (summarised from Tables 3–5). The volume percentages of mixed-layer clay and kaolinite are only listed for comparison since they are not corrected for microporosity.

	Campanian channel sandstones (vol-%)		Post-Campanian channel sandstones (vol-%)	
	Range	Average	Range	Average
Mixed-layer clay	6.5–13.5	10.1	<1	<1
Kaolinite	0.0–0.5	0.1	0.0–0.5	0.3
Quartz	5.0–12.5	7.6	0.0–2.0	1.1
Ankerite	0.0–3.0	0.7	0.5–1.7	0.9
Porosity	1.0–4.5	2.6	10.8–22.3	17.3

The increased amount of mixed-layer clay observed in the Campanian sandstones may be related to illitisation of detrital clay (Boles & Franks 1979). Pressure solution is rather insignificant in the GANT#1 sandstones. Alternatively, rapid burial during active volcanism could be a possible explanation for precipitation of 3rd generation quartz overgrowths. Storey *et al.* (in press) suggest that the Paleocene volcanic package erupted very fast during a period of 1 million years or less and according to McBride (1989) most quartz in rapidly subsiding basins precipitate by cooling of ascending formation waters generated at greater depth. It is unclear to what extent precipitation of 3rd generation

quartz is controlled by rapid burial, but the different amounts of quartz in the Campanian and Maastrichtian–Paleocene sandstones suggest that either time or depth of burial was a controlling factor. The timing of Mg-siderite type 3 growth relative to 3rd generation quartz and ankerite is unknown in the GANT#1 core but late Mg-siderite has been reported to predate ankerite elsewhere (MacAulay *et al.* 1993). The chemical composition of Mg-siderite type 3 in GANT#1 strongly suggests a marine origin without influence of meteoric waters (cf. Mozley 1989). Ankerite precipitating subsequent to 3rd generation quartz overgrowths formed the latest, generally occurring cementing phase and is probably related to a release of iron and magnesium from decomposing smectite in the mudstones during burial diagenesis (Boles 1978; Kantorowicz 1985).

The Maastrichtian–Paleocene burial thus initiated with compaction and precipitation of minerals from evolved marine waters during shallow burial leading to a deeper stage of burial characterised by alterations within mudstones which effectively changed the porewater chemistry in the sandstones. The shift from shallow to deep burial is marked by a gain in mechanical stability and the onset of feldspar dissolution driven by decomposition of organic matter in mudstones. Deep burial is characterised by initial formation of secondary porosity due to feldspar dissolution followed by a reduction of porosity by precipitation of minerals which are probably related to diagenetic changes in mudstone clay mineralogy at greater depth of burial.

Reservoir conditions

Conventional core analyses on 19 plugs from GANT#1 revealed a range in porosity from 0,60 to 17,45% and in permeability from 0,007 to 33,8 mD (Table 8). The permeability is generally low (<10 mD) but the porosity of the post-Campanian sandstones is slightly increased compared to Campanian sandstones. Although only a limited number of analyses are available they seem to represent the general quality of sandstones in the well based on the inspection of 72 thin sections. Two less lithified sandstone units were encountered during sampling for thin sections. These units are ~12 m thick and located in the upper part of Maastrichtian submarine canyon conglomerate unit in the intervals 160–171 m and 180–192 m (for details, see Dam 1996: sheets “48 of 60”–“50 of 60”). Analyses of five samples from these units reveal porosities varying from 12,11 to 18,79% and permeabilities varying from 16,6 to 90,7 mD (Table 8). The GANE#1 and GANE#1A wells on the south coast of Nuussuaq provide a section through Upper Paleocene turbiditic sandstone units encased in mudstone which thus furnish complementary and stratigraphically higher sections to that found in GANT#1. However, porosities and permeabilities of the GANE#1 and GANE#1A cores are low with an arithmetic average of 6.5% and 1.46 mD, respectively (Andersen 1996).

The sandstones of the GANT#1 core classify as subarkoses but the Maastrichtian–Paleocene succession is slightly more mature than the channel sandstones from the Campanian succession (Fig. 2). Interchannel sandstones are slightly more mature than channel sandstones but have experienced the same diagenetic alterations and are thus treated equally ignoring variations in depositional environment. From thin sections it is estimated that the sandstones are generally poorly sorted but that the Maastrichtian–Paleocene sandstones are slightly better sorted than the Campanian sandstones. Notably, the coarse-grained post-Campanian sandstones contain relatively little, if any detrital clay.

Mudstone clasts which are strongly deformed occur in very different amounts but are generally more abundant in the Maastrichtian–Paleocene sandstones than in the Campanian sandstones (Table 1). Plant debris, which is most abundant in Campanian sandstones, has a similar elongated shape as muscovite and is bent around rigid grains. Mica which is also deformed due to compaction is more abundant in the Campanian than in the post-Campanian sandstones (Table 1). The mentioned differences in detrital composition may represent a shift in provenance which could explain the apparent lack of oligoclase in the post-Campanian sandstones.

Most of the present porosity is secondary originating from dissolution of detrital feldspar grains which resulted in skeletal grains, isolated moulds and grain surface corrosion; the following growth of kaolinite, albite, quartz, siderite and ankerite all reduced this porosity. Formation of secondary porosity may not significantly have raised permeability, which is a function of the abundance of intergranular macroporosity (Ehrenberg 1990), since most feldspar dissolution porosity in GANT#1 seems to be intragranular.

There is a marked difference in the degree of cementation between the Campanian and post-Campanian channel sandstones as the Campanian contain relatively high amounts of mixed-layer clay and quartz (Table 9). The difference in cementation of the Campanian and post-Campanian sandstones is paralleled by a difference in measured porosity and permeability (Table 10). Campanian

sandstones have an average porosity of 7.8% and permeabilities less than 10 mD, whereas the Maastrichtian–Paleocene sandstones have an average porosity of 12.7% and somewhat better permeabilities between 10 and 100 mD.

Table 10. Range of porosities and permeabilities (perm.) for Campanian and Maastrichtian–Paleocene sandstones measured by conventional core analysis.

	Campanian sandstones		Post-Campanian sandstones	
	Porosity (%)	Gas perm. (mD)	Porosity (%)	Gas perm. (mD)
Conventional core analysis	4.92–13.73	0.106–4.05	5.21–17.45	0.112–33.8
Spot-analysis			12.11–18.79	16.6–90.7

A slight, but distinct difference in reservoir quality is thus observed between Maastrichtian–Paleocene and Campanian sandstones but the actual cause for this difference is somewhat speculative taking the difference in grain size, grain types, sorting, maturity, difficulties in exact differentiations between early and late quartz cement, and between secondary and primary porosity into account.

It is notable that although the post-Campanian sandstones contain only minor amounts of cement permeabilities do not exceed 100 mD implying that detritus is a major control on reservoir quality. This is supported by the poor sorting of the sediment which reduces both porosity and permeability (Beard & Weyl 1973) and the content of ductile mudstone clasts and siderite aggregates which increase the degree of mechanical compaction (Pittman & Larese 1991). The amount of intraformational siderite aggregates varies strongly but generally does not exceed 10% by volume although it may reach up to 25–40% by volume in some samples. Both siderite aggregates and mudstone clasts are deformed due to compaction and have developed a characteristic flame-structured pseudomatrix (cf. Dickinson 1970). According to (Ehrenberg & Boassen 1993) illitic clay may control pore-size distribution and abundance of intergranular macroporosity (i.e. permeability) but since similar clays are virtually absent in the post-Campanian sandstones in GANT#1 they are not of major importance.

As a qualitative model it is thus proposed that the rather poor reservoir quality generally characterising the sandstones of the GANT#1 core mainly results from compaction of a poorly sorted sediment containing ductile clasts combined with precipitation of minor amounts of diagenetic minerals during shallow burial reducing primary porosity. Furthermore, the secondary, intragranular porosity developed through dissolution of feldspars during deeper burial was reduced by later diagenetic stages.

Conclusions

1. A general model for the diagenetic changes in GANT#1 involves progressive, shallow burial during the Campanian in a marine, eogenetic environment characterised by evolved marine porewaters which precipitated apatite, pyrite, siderite, quartz and mixed-layer clay. This was followed by a relative sea-level fall giving access for meteoric dominated pore water and formation of ferroan carbonate concretionary zones. During this diagenetic stage the sediments were only very slightly compacted due to the shallow burial. Following renewed deposition the total package of Cretaceous and Paleocene sediments was affected by further compaction and diagenetic changes. High rates of sedimentation are suggested by microfracturing of rigid detrital grains. The loss of primary porosity in the sandstones due to compaction is believed largely to depend on poor sorting and the character of the detritus, especially the high content of ductile constituents. Compaction is followed by a deeper stage of burial characterised by alterations within mudstones which effectively changed the porewater chemistry in the sandstones. This caused formation of secondary porosity to develop due to feldspar dissolution. The secondary porosity was, however, reduced by later diagenetic phases.
2. Most of the sandstones in GANT#1 classify as subarkoses but general compositional differences, and in particular the lack of oligoclase in the post-Campanian sandstones, suggest a supply of more mature sediments in the Maastrichtian–Paleocene than in the Campanian.
3. Reservoir properties of the turbiditic sandstone intervals in both the GANT#1 and GANE#1 wells are generally relatively poor. This is primarily due to the detrital composition of the sandstones (especially the high content of ductile constituents) and the overall poor sorting and not to cementation.
4. Although the reservoir properties of the sandstone intervals in the GANT#1 and GANE#1 wells are generally relatively poor, it is suggested that moderate to good properties may be found in certain intervals within the Maastrichtian–Paleocene succession. However, the reason for the locally enhanced reservoir properties in GANT#1 was not clarified by this study partly due to the lack of regional petrographical data.

References

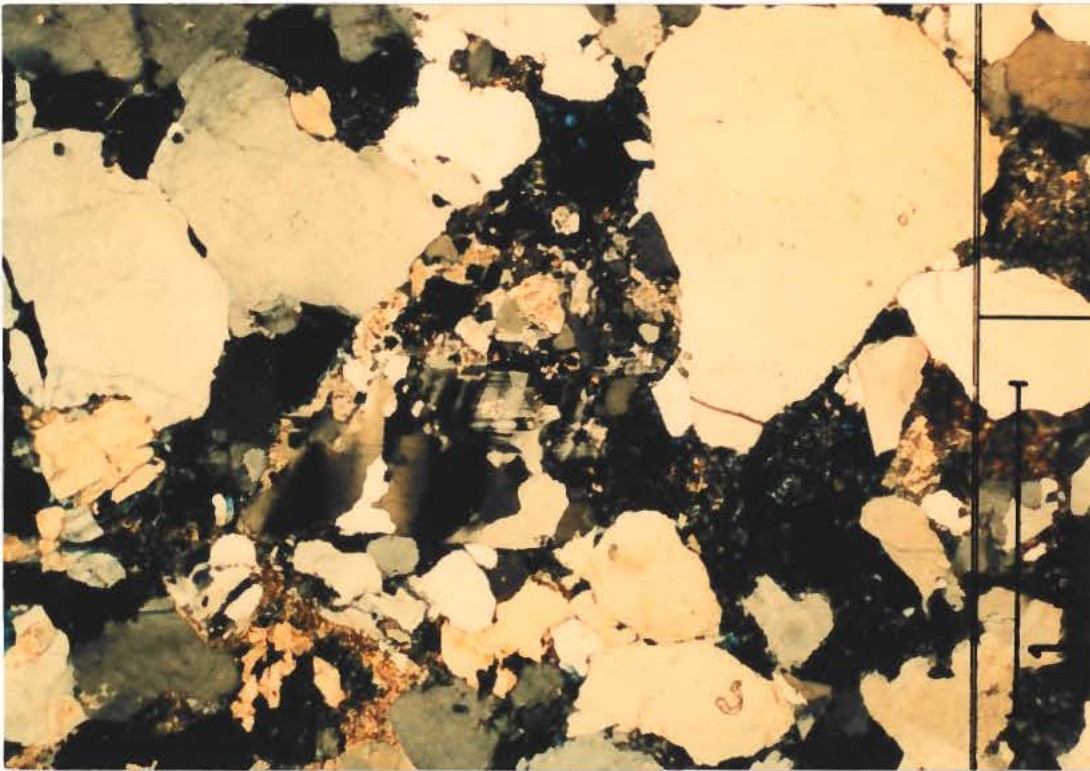
- Allan, J.R. & Matthews, R.K. 1977: Carbon and oxygen isotopes as diagenetic and stratigraphic tools: surface and subsurface data, Barbados, West Indies. *Geology* **5**(1), 16–20.
- Andersen, G. 1996: Conventional core analysis on GANE#1 and GANE#1A cores, Eqaulluk, Nuussuaq, West Greenland. *Danmarks og Grønlands Geologiske Undersøgelse Rapport* **1996/117**, 35 pp.
- Beard, D.C. & Weyl, P.K. 1973: Influence of texture on porosity and permeability of unconsolidated sand. *American Association of Petroleum Geologists Bulletin* **57**(2), 349–369.
- Berner, R.A. 1984: Sedimentary pyrite formation: an update. *Geochimica et Cosmochimica Acta* **48**(4), 605–615.
- Bjørlykke, K. & Aagaard, P. 1992: Clay minerals in North Sea sandstones. diagenesis and petrophysics of clay minerals in sandstones. In: Houseknecht, D.W. & Pittman, E.D. (eds): *Origin, diagenesis, and petrophysics of clay minerals in sandstones*. Society of Economic Paleontologists and Mineralogists Special Publication **47**, 65–80.
- Boles, J.R. 1978: Active ankerite cementation in the subsurface Eocene of Southwest Texas. *Contributions to Mineralogy and Petrology* **68**(1), 13–22.
- Boles, J.R. & Franks, S.G. 1979: Clay diagenesis in the Wilcox sandstones of southern Texas: Implications of smectite diagenesis on sandstone cementation. *Journal of Sedimentary Petrology* **49**(1), 55–70.
- Boles, J.R. & Johnson, K.S. 1984: Influence of mica surfaces on pore-water pH. *Chemical Geology* **43**(3–4), 303–317.
- Burley, S.D., Kantorowicz, J.D. & Waugh, B. 1985: Clastic diagenesis. In: Brenchley, P.J.W. & Williams, B.P.J. (eds): *Sedimentology: Recent developments and applied aspects*. Geological Society Special Publication **18**, 189–220. London: Geological Society.
- Chalmers, J.A., Pulvertaft, T.C.R., Christiansen, F.G., Larsen, H.C., Laursen, K.H. & Ottesen, T.G. 1993: The southern West Greenland continental margin: rifting history, basin development and petroleum potential. In: Parker, J.R. (ed.): *Petroleum geology of northwest Europe: proceedings of the 4th conference*, 915–931. London: Geological Society.
- Christiansen, F.G., Bojesen-Koefoed, J., Nytoft, H.-P. & Laier, T. 1996: Organic geochemistry of sediments, oils, and gases in the GANE#1, GANT#1 and GANK#1 wells, Nuussuaq, West Greenland. *Danmarks og Grønlands Geologiske Undersøgelse Rapport* **1996/23**, 35 pp.
- Dam, G. 1996: Sedimentology of the GANT#1 core drilled by grønArctic Energy Inc., Tunorsuaq, Nuussuaq, West Greenland. *Danmarks og Grønlands Geologiske Undersøgelse Rapport* **1996/96**, 18 pp.
- Dam, G. & Sønderholm, M. 1998: Sedimentological evolution of a fault-controlled Early Paleocene incised valley system, Nuussuaq Basin, West Greenland. In: Shanley, K.W. & McCabe, P.J. (eds): *Relative role of eustasy, climate, and tectonism in continental rocks*. Society of Economic Paleontologists and Mineralogists Special Publication **59**.
- Deer, W.A., Howie, R.A. & Zussman, J. 1992: *An introduction to the rock-forming minerals*, 2nd edition, 696 pp. Essex: Longman Scientific & Technical.
- Dickinson, W.R. 1970: Interpreting detrital modes of graywacke and arkose. *Journal of Sedimentary Petrology* **40**(2), 695–707.
- Dutton, S.P. & Land, L.S. 1985: Meteoric burial diagenesis of Pennsylvanian arkosic sandstones, Southwestern Anadarko Basin, Texas. *American Association of Petroleum Geologists Bulletin* **69**(1), 22–38.

- Ehrenberg, S.N. 1990: Relationship between diagenesis and reservoir quality in sandstones of the Garn Formation, Haltenbanken, Mid-Norwegian Continental Shelf. *American Association of Petroleum Geologists Bulletin* **74**(10), 1538–1558.
- Ehrenberg, S.N. 1991: Kaolinized, potassium-leached zones at the contacts of the Garn Formation, Haltenbanken, mid-Norwegian continental shelf. *Marine and Petroleum Geology* **8**(3), 250–269.
- Ehrenberg, S.N. & Boassen, T. 1993: Factors controlling permeability variations in sandstones of the Garn Formation in the Trestakk Field, Norwegian continental shelf. *Journal of Sedimentary Petrology* **63**(5), 929–944.
- Esposito, K.J. & Whitney, G. 1995: Thermal effects of thin igneous intrusions on diagenetic reactions in a Tertiary basin of southwestern Washington. *United States Geological Survey Bulletin* **2085-C**, 40 pp.
- Fisher, R.S. & Land, L.S. 1986: Diagenetic history of Eocene Wilcox sandstones, south-central Texas. *Geochimica et Cosmochimica Acta* **50**(4), 551–561.
- Folk, R.L. 1968: *Petrology of sedimentary rocks*, 170 pp. Austin, Texas: Hemphill's.
- Gautier, D.L., Kharaka, Y.K. & Surdam, R.C. 1985: Relationship of organic matter and mineral diagenesis. *Society of Economic Paleontologists and Mineralogists Short Course* **17**, 279 pp.
- Glenn, C.R. & Arthur, M.A. 1988: Petrology and major element geochemistry of Peru margin phosphorites and associated diagenetic minerals: authigenesis in modern organic-rich sediments. *Marine Geology* **80**(3–4), 231–267.
- Kantorowicz, J.D. 1985: The origin of authigenic ankerite from the Ninian Field, UK North Sea. *Nature* **315**(6016), 214–216.
- Kierkegaard, T. 1997: *Petrografi og diagenese: GANT#1 boringen, Tunorsuaq, Nuussuaq, Vestgrønland*. Unpublished M. Sc. thesis, Aarhus Universitet, Århus, Denmark, 99 pp.
- Larsen, L.M., Pedersen, A.K. & Dalhoff, F. in press: Oil impregnations in Paleocene hyaloclastites and lava flows in the Nuussuaq Basin, central West Greenland. Cores from the Northwest European hydrocarbon province: 1997 volume London: Geological Society.
- Longstaffe, F.J. & Ayalon, A. 1987: Oxygen-isotope studies of clastic diagenesis in the Lower Cretaceous Viking Formation, Alberta: implications for the role of meteoric water. In: James, M.D. (ed.): *Diagenesis of sedimentary sequences*. Geological Society Special Publication **36**, 277–296. London: Geological Society.
- MacAulay, C.I., Haszeldine, R.S. & Fallick, A.E. 1993: Distribution, chemistry, isotopic composition and origin of diagenetic carbonates: Magnus sandstone, North Sea. *Journal of Sedimentary Petrology* **63**(1), 33–43.
- McBride, E.F. 1989: Quartz cement in sandstones; a review. *Earth-Science Reviews* **26**(2), 69–112.
- Mozley, P.S. 1989: Relation between depositional environment and the elemental composition of early diagenetic siderite. *Geology* **17**(8), 704–706.
- Mozley, P.S. & Burns, S.J. 1993: Oxygen and carbon isotopic composition of marine carbonate concretions: an overview. *Journal of Sedimentary Petrology* **63**(1), 73–83.
- Nøhr-Hansen, H. 1997: Palynology of the boreholes GANE#1, GANK#1 and GANT#1 Nuussuaq, West Greenland. *Danmarks og Grønlands Geologiske Undersøgelse Rapport* **1997/89**, 22 pp.
- Nøhr-Hansen, H. & Dam, G. 1997: Palynology and sedimentology across a new marine Cretaceous/Tertiary boundary section on Nuussuaq, West Greenland. *Geology* **25**(9), 851–854.
- Pittman, E.D. & Larese, R.E. 1991: Compaction of lithic sands: experimental results and applications. *American Association of Petroleum Geologists Bulletin* **75**(8), 1279–1299.

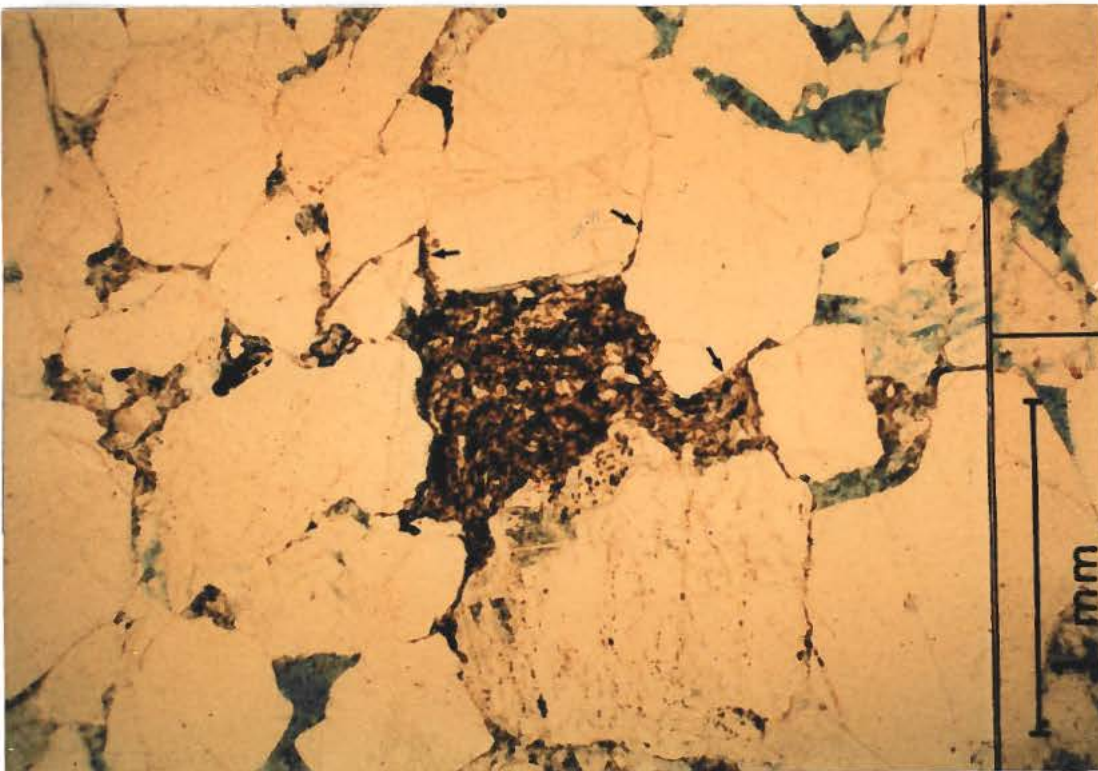
- Rolle, F. 1985: Late Cretaceous–Tertiary sediments offshore central West Greenland: Lithostratigraphy, sedimentary evolution, and petroleum potential. *Canadian Journal of Earth Sciences* **22**(7), 1001–1019.
- Rosenkrantz, A. 1970: Marine Upper Cretaceous and lowermost Tertiary deposits in West Greenland. *Meddelelser fra Dansk Geologisk Forening* **19**(4), 406–453.
- Storey, M., Duncan, R.A., Pedersen, A.K., Larsen, L.M. & Larsen, H.C. in press: $^{40}\text{Ar}/^{39}\text{Ar}$ geochronology of the West Greenland Tertiary volcanic province. *Earth and Planetary Science Letters*.
- Surdam, R.C., Crossey, L.J., Hagen, E.S. & Haesler, H.P. 1989: Organic-inorganic interactions and sandstone diagenesis. *American Association of Petroleum Geologists Bulletin* **73**(1), 1–23.
- van der Plas, L. & Tobi, A.C. 1965: A chart of judging the reliability of point counting results. *American Journal of Science* **263**(1), 87–90.
- Wilson, M.D. & Pittman, E.D. 1977: Authigenic clays in sandstones: Recognition and influence on reservoir properties and paleoenvironmental analysis. *Journal of Sedimentary Petrology* **47**(1), 3–31.

Plates

1

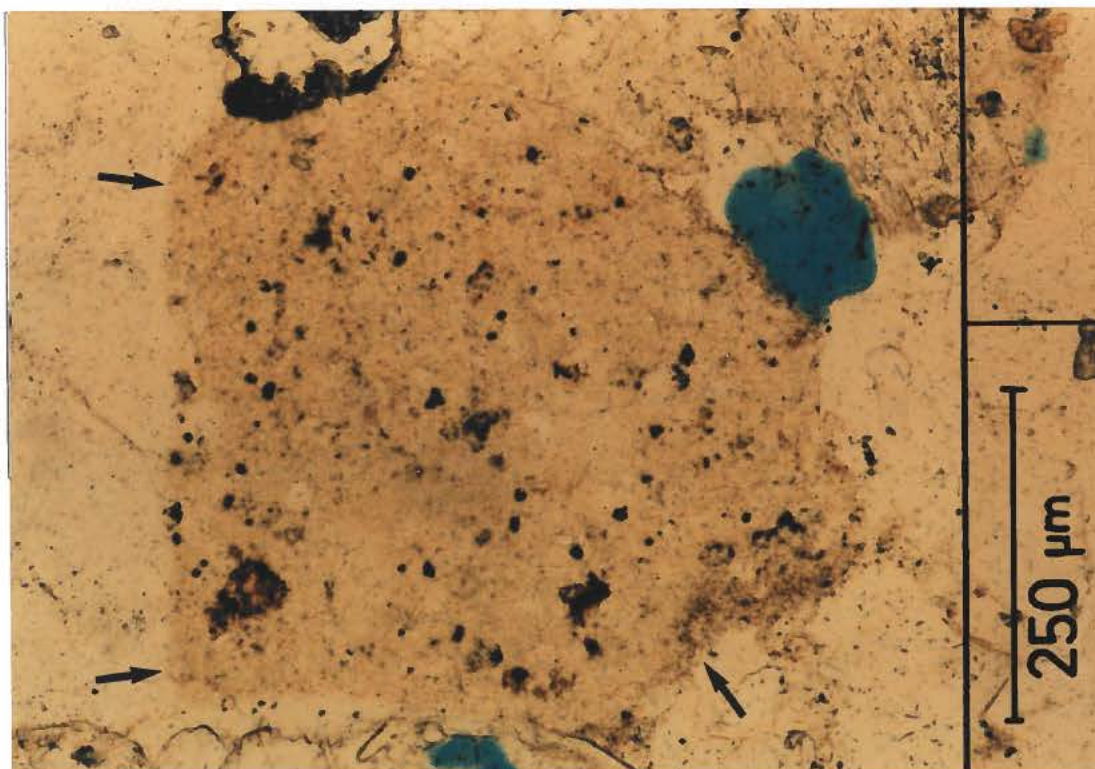


2

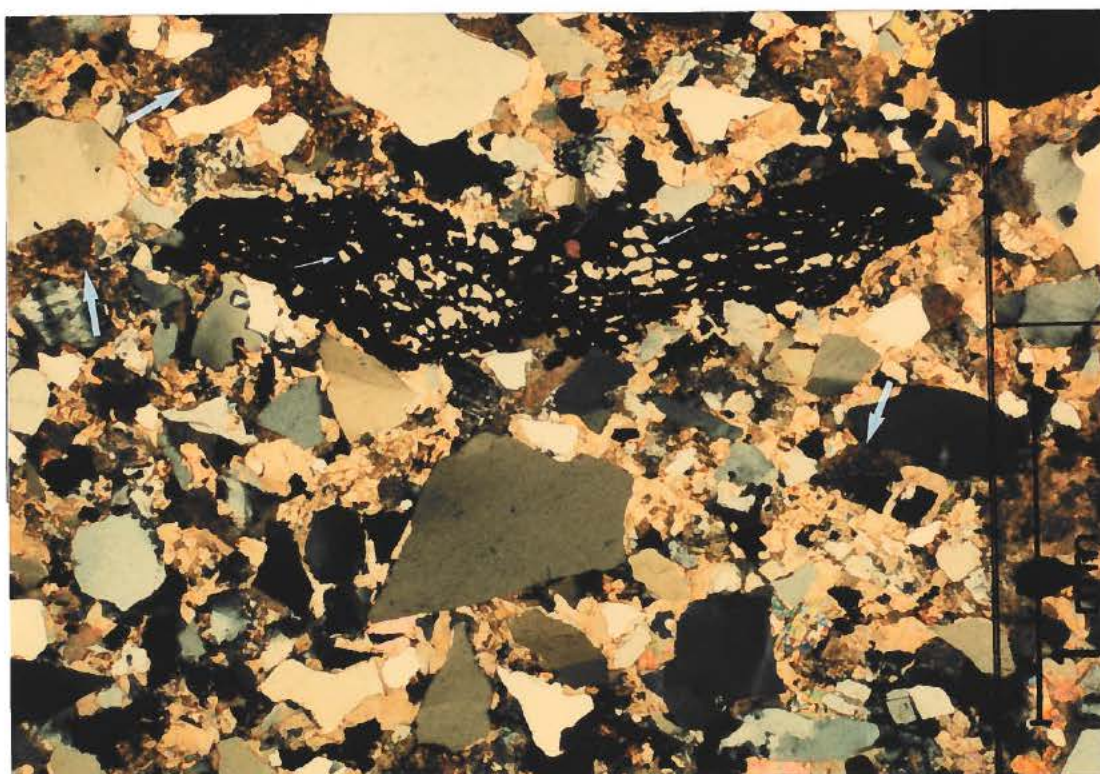


1. Rock fragment of quartz and feldspar crystals containing some ankerite.
2. Deformed mudstone clast. Arrow points at pseudomatrix.

1



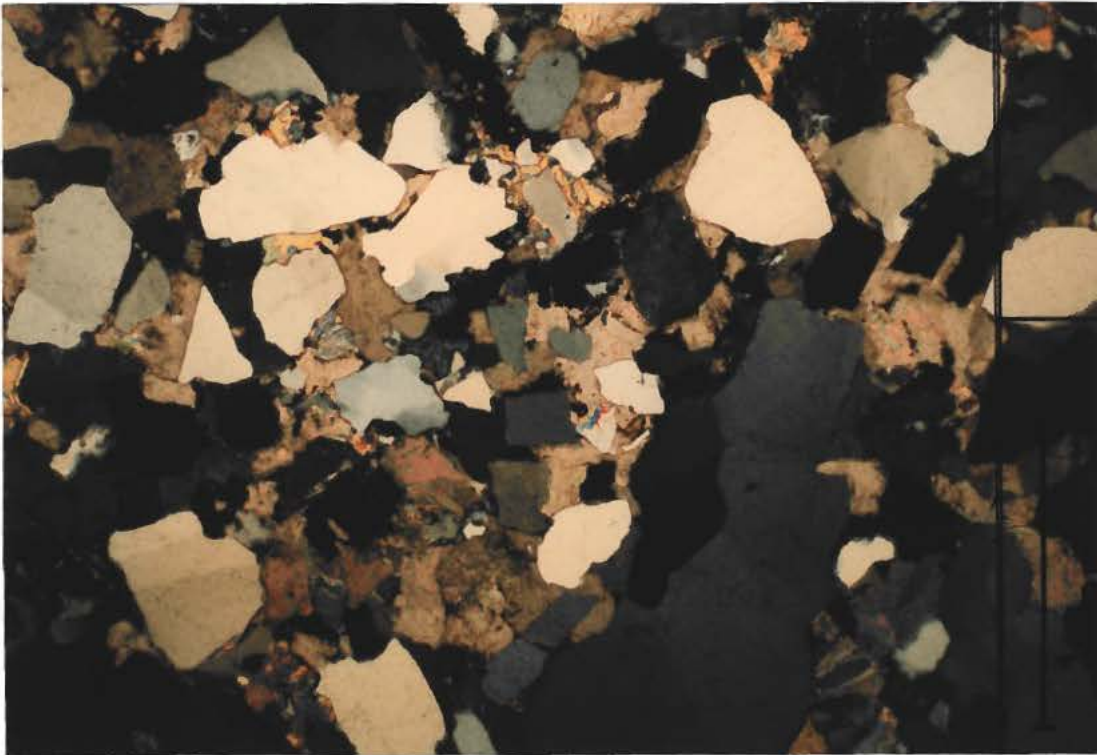
2



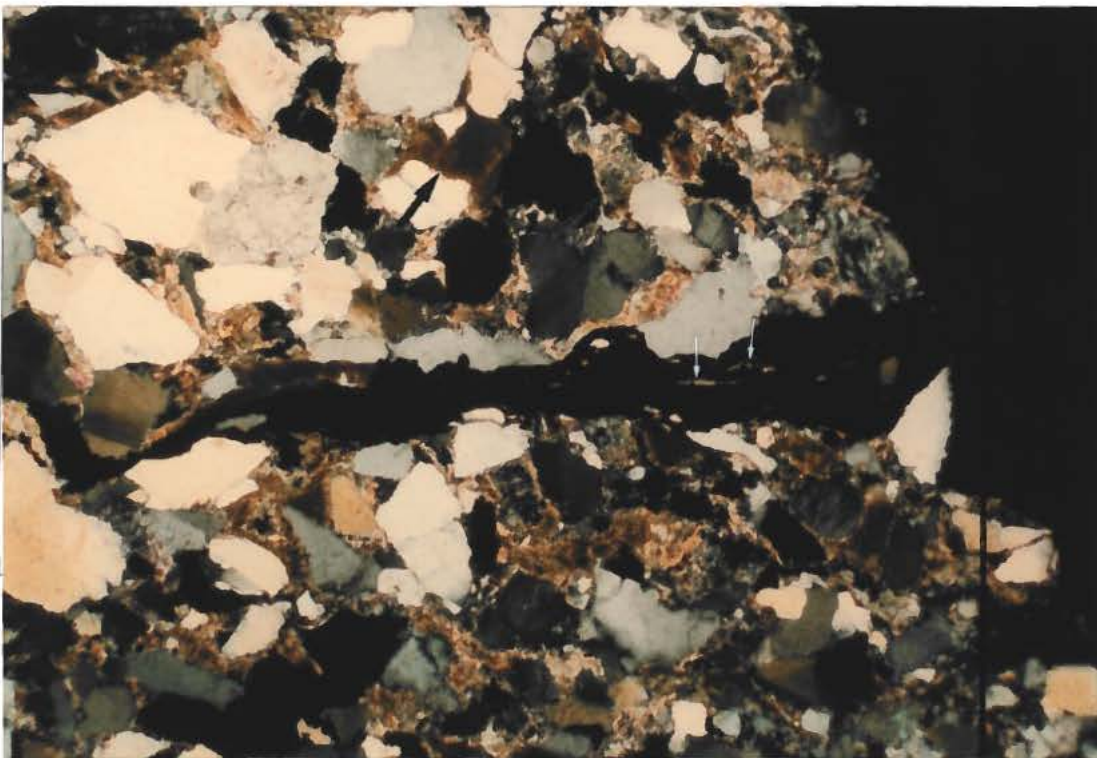
1. Chert grain.

2. Porous plant debris within a concretionary zone. Micropores are filled with ferroan carbonate stabilising the plant debris against compaction.

1

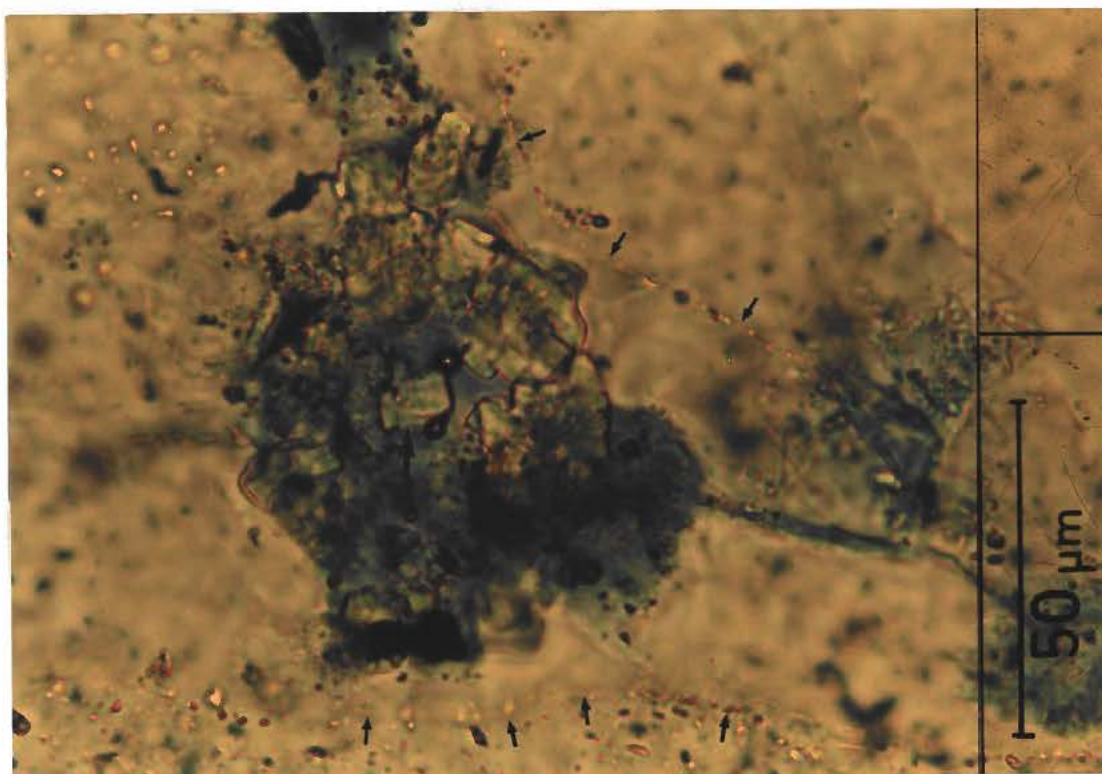


2

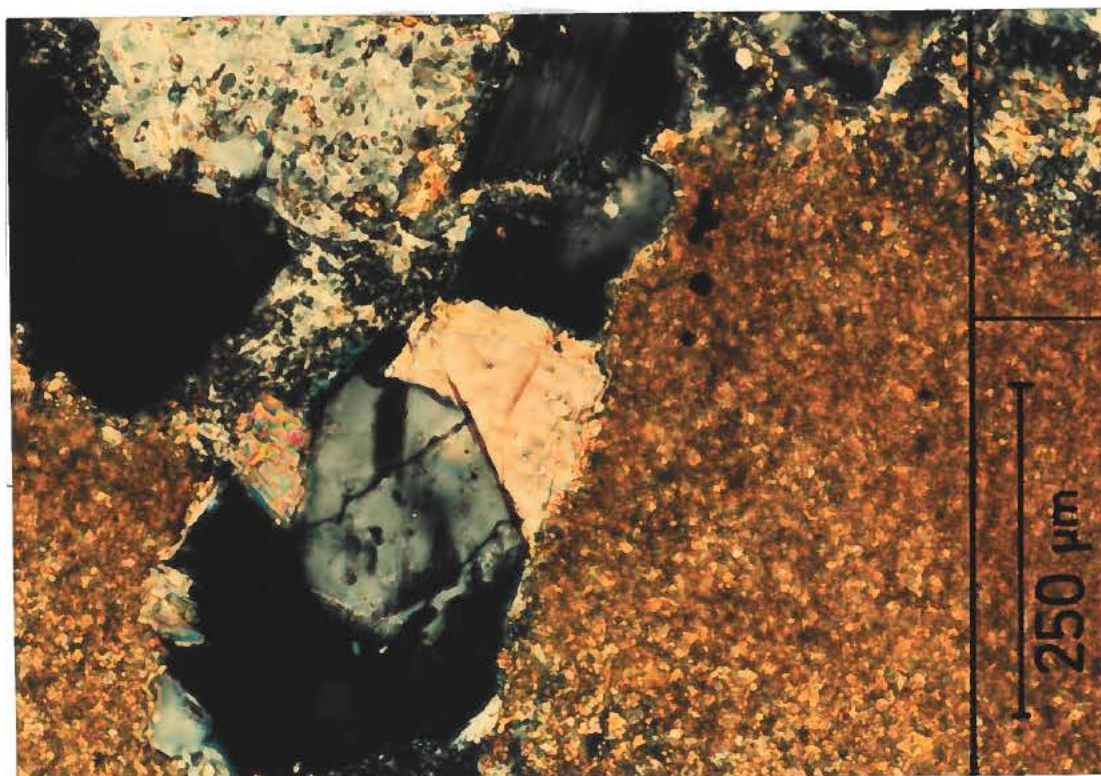


1. Framework detrital floating in a concretionary cement. Note large minus-cement porosity.
2. Strongly deformed plant debris within an uncemented sandstone next to a concretionary zone. Almost all internal microporosity is obliterated before cementation with ankerite (small arrows). Note the strongly deformed siderite aggregate (large arrow).

1



2

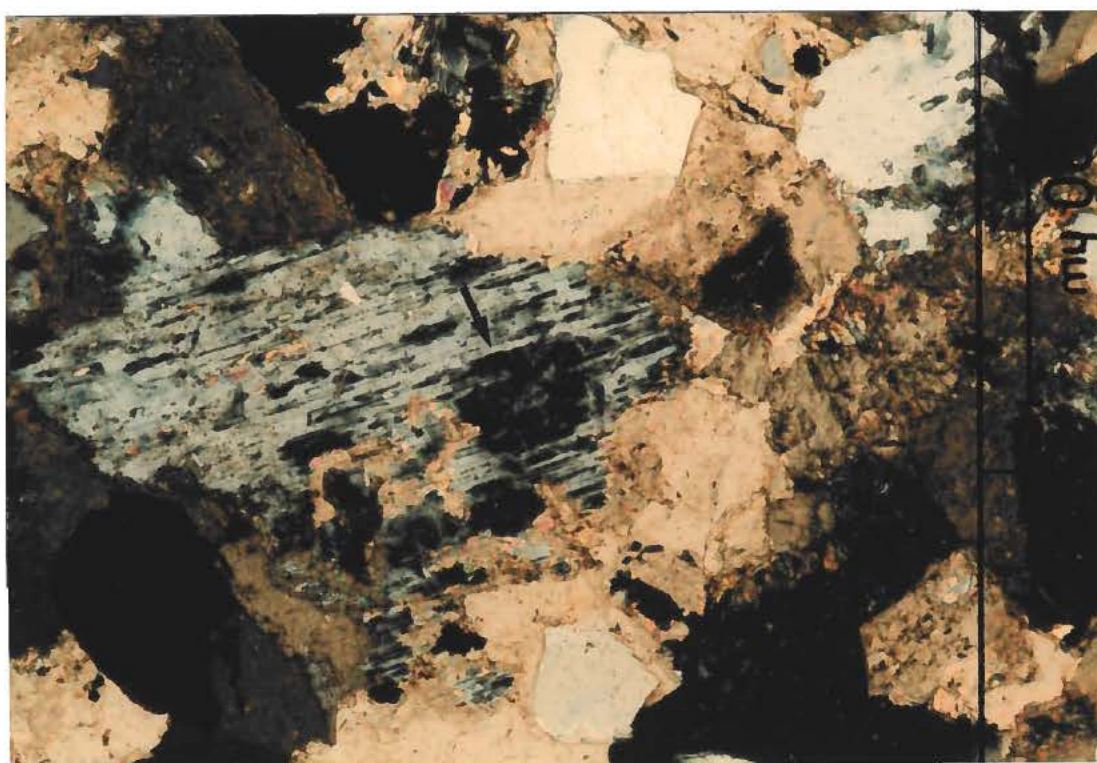


1. Cluster of apatite crystals. Large arrow point on a single crystal. The crystals on this Plate are partly encapsulated but single crystals are often completely encapsulated. A quartz overgrowth is outlined by small arrows.
2. Deformed siderite aggregate with flame structure, see also Plate 13.5. The outer parts of the flames are cut off into pseudomatrix.

1



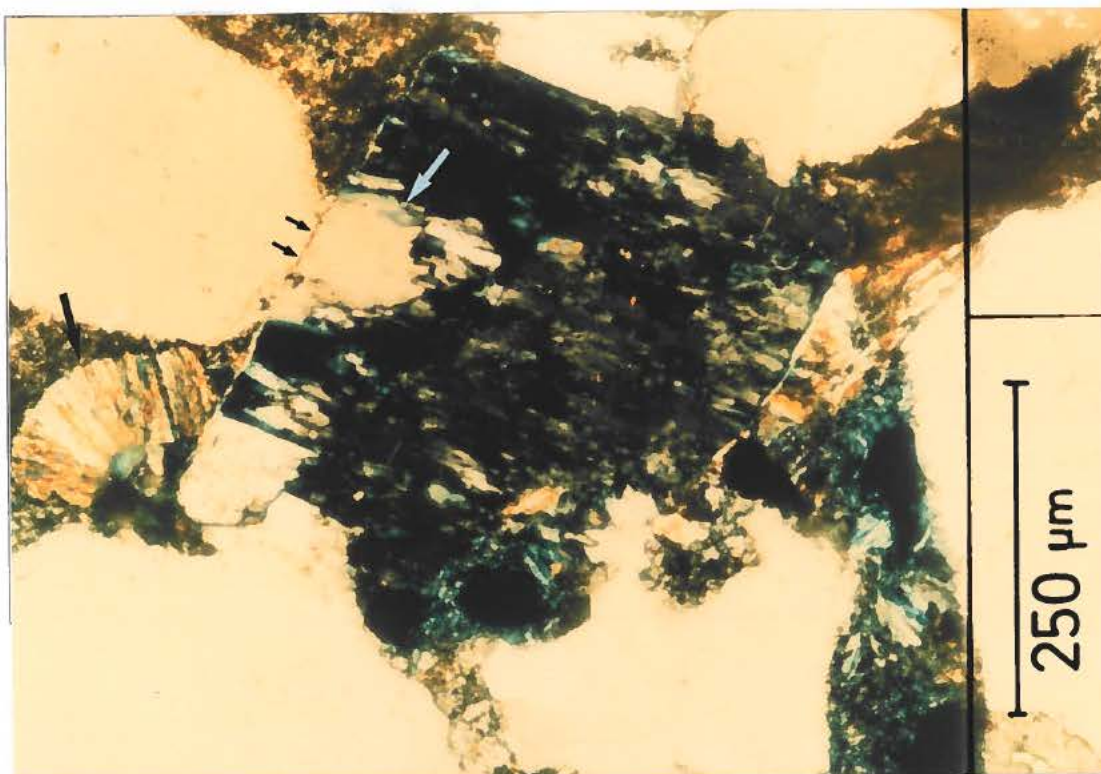
2



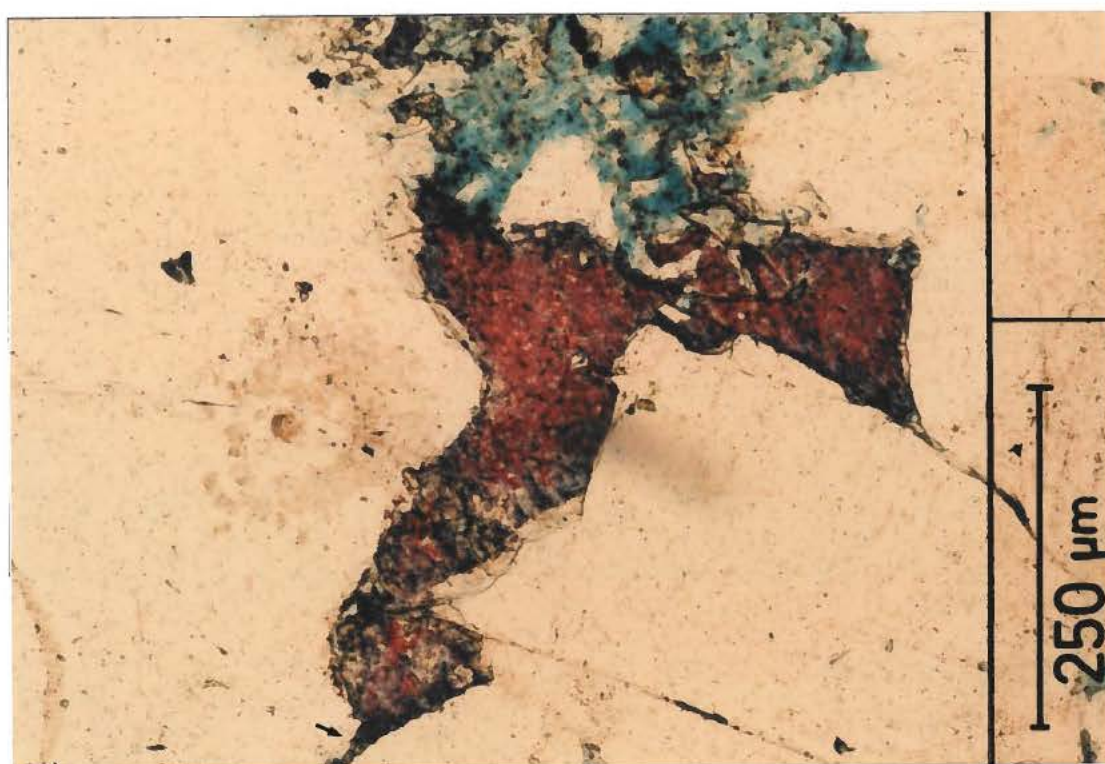
1. Microcrystalline siderite aggregate. Note difficulty in recognising the clay content of in the aggregates, see also Plate 13.5.

2. Feldspar grain within a concretionary zone which is partly replaced with kaolinite.

1

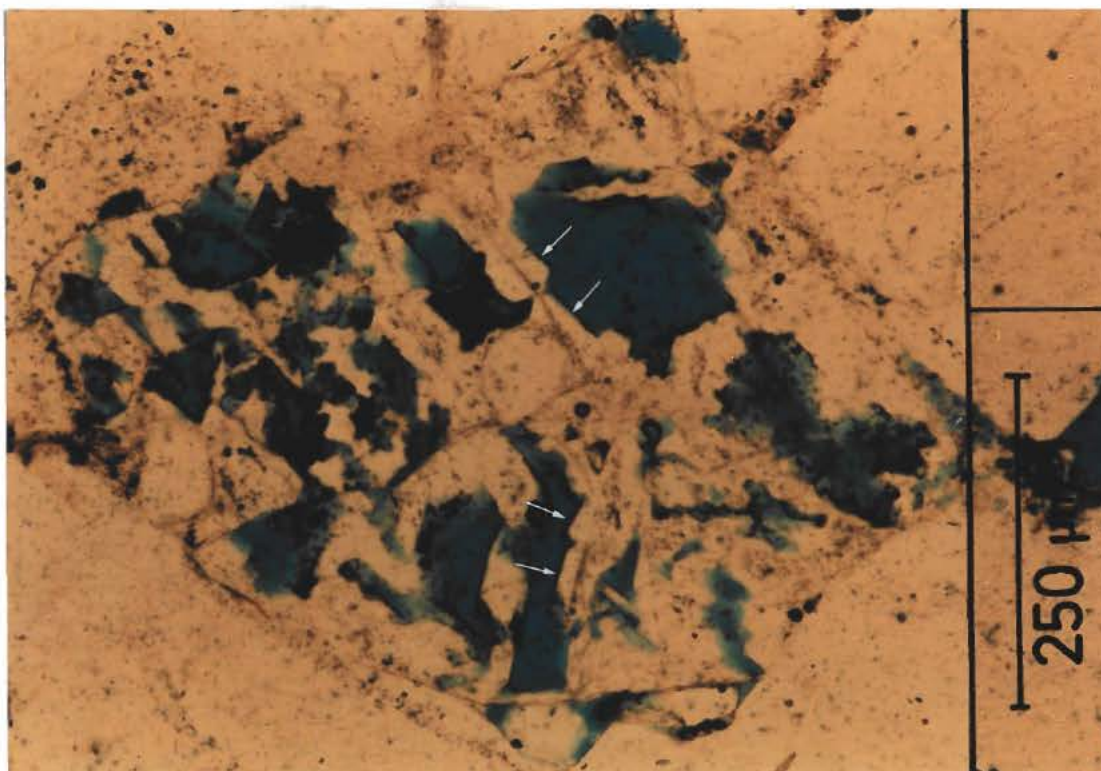


2

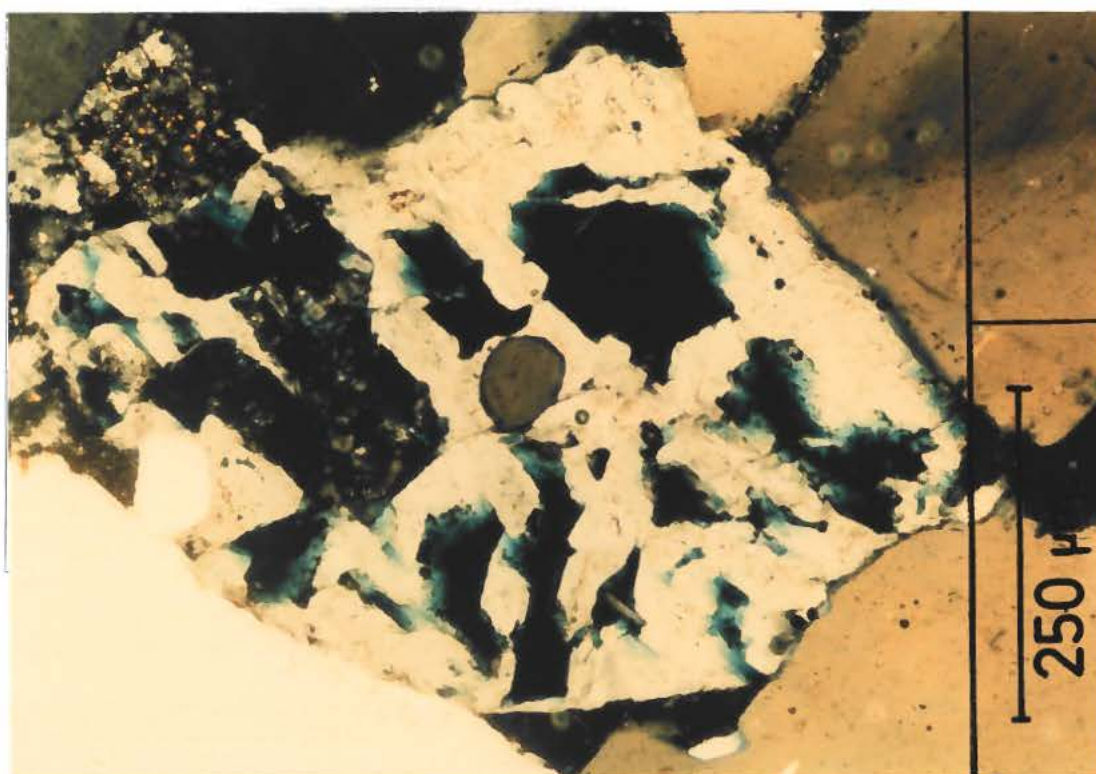


1. Skeletal feldspar grain infilled by 3rd generation quartz. Mixed-layer clay rim do not enter the secondary porosity indicating that feldspar dissolution post-dates formation of clay rims. Since 3rd generation quartz occurs within secondary porosity it post-dates feldspar dissolution. The outline of the feldspar grain is intact although it is almost completely dissolved indicating that dissolution occurred after the sandstone was mechanically stable.
2. Porefilling calcite (red upon staining) which is more bluish in its marginal parts. A small quartz overgrowth is covered by the calcite (arrow).

1

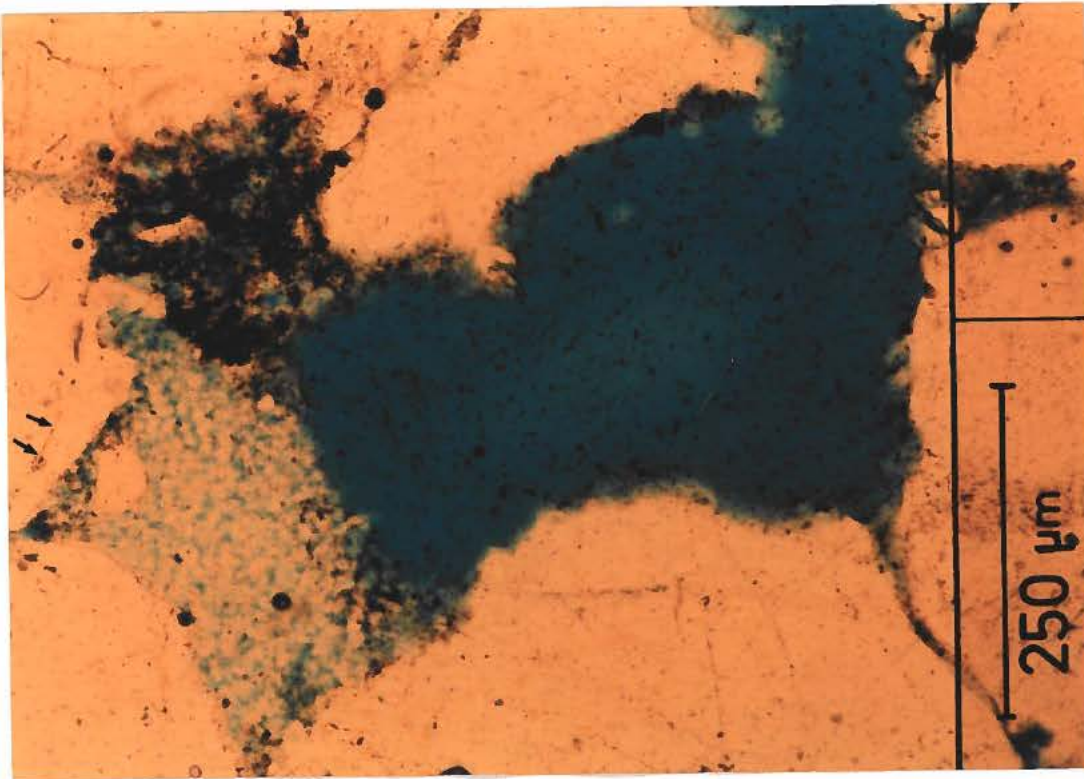


2

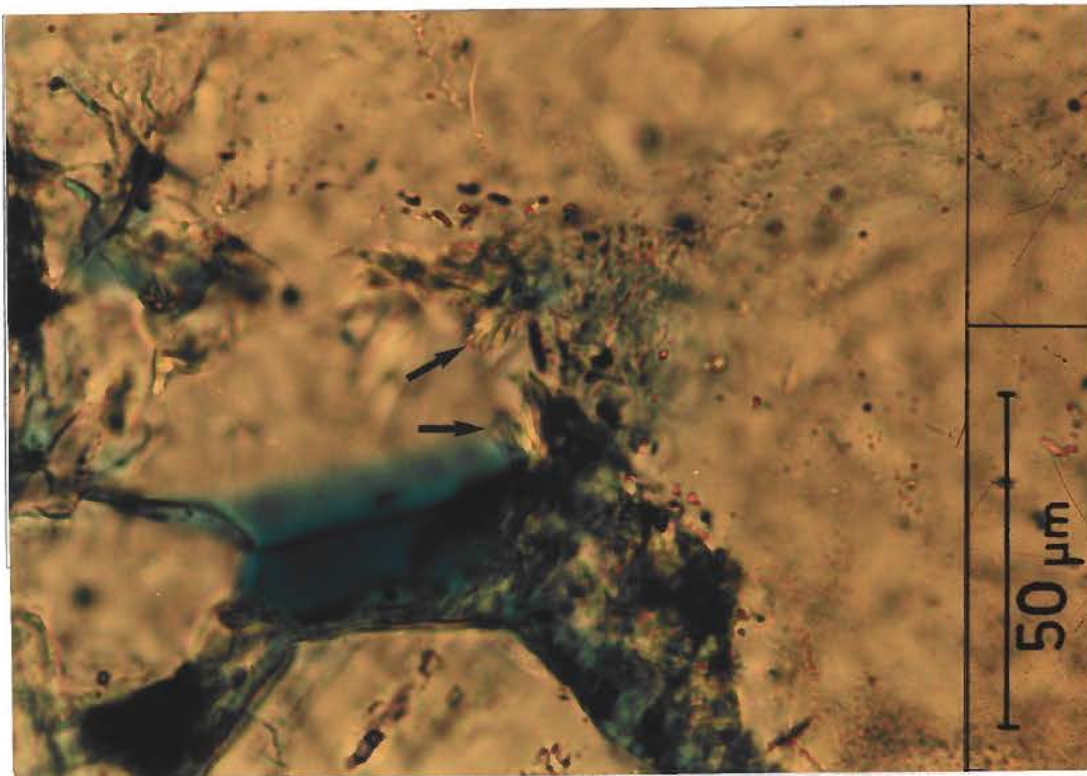


1. Euhedral albite crystal nucleating on dissolution remnants.
2. Same as Plate 7.1 but with crossed nicols. Note uniform extinction.

1

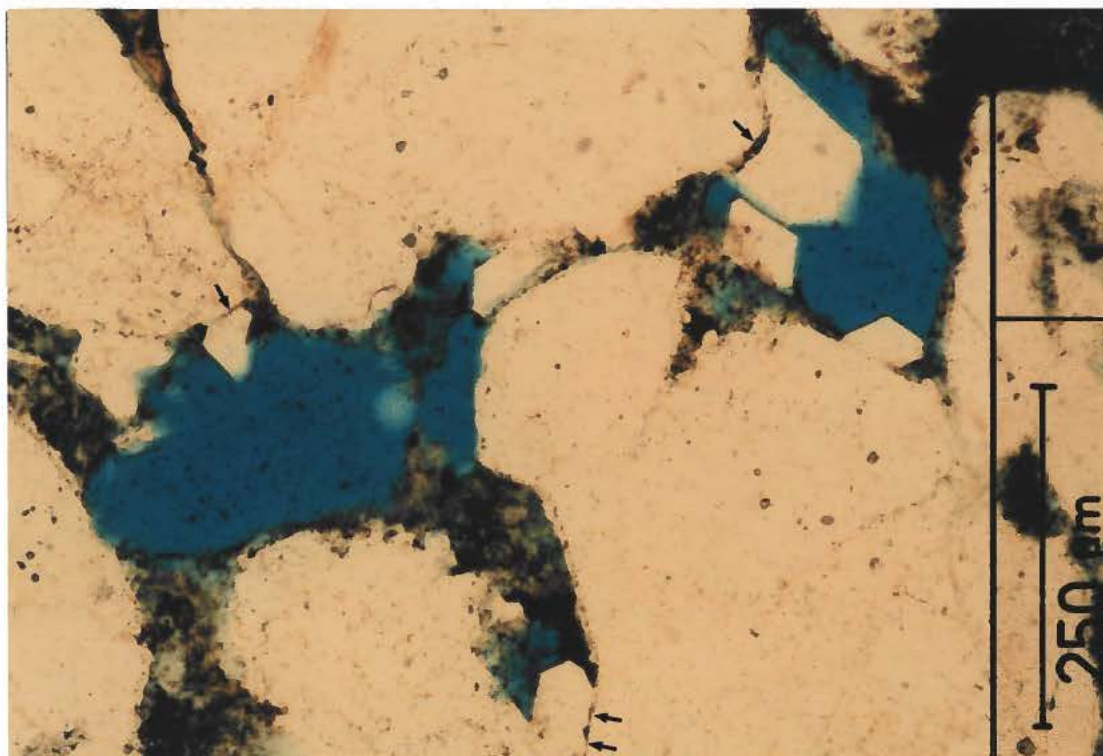


2

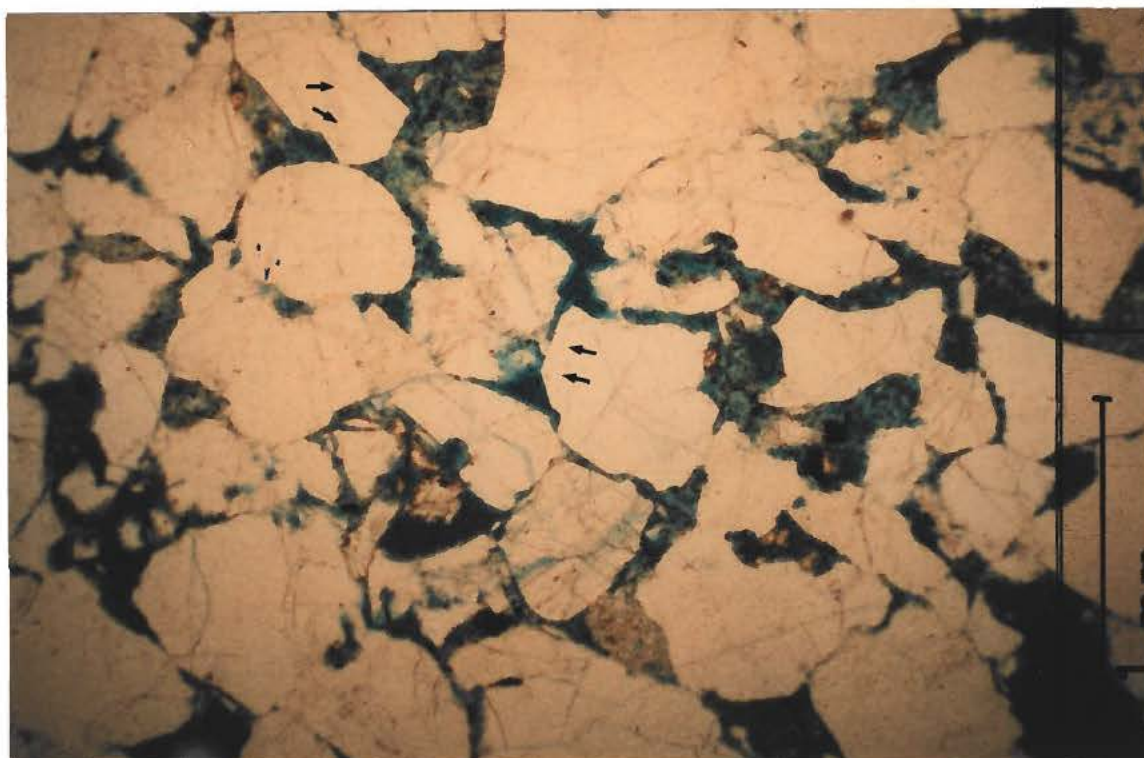


1. Aggregate of kaolinite booklets next to moldic porosity. The kaolinite precipitated before the formation of moulds.
2. Chlorite fans encapsulated by quartz overgrowths.

1

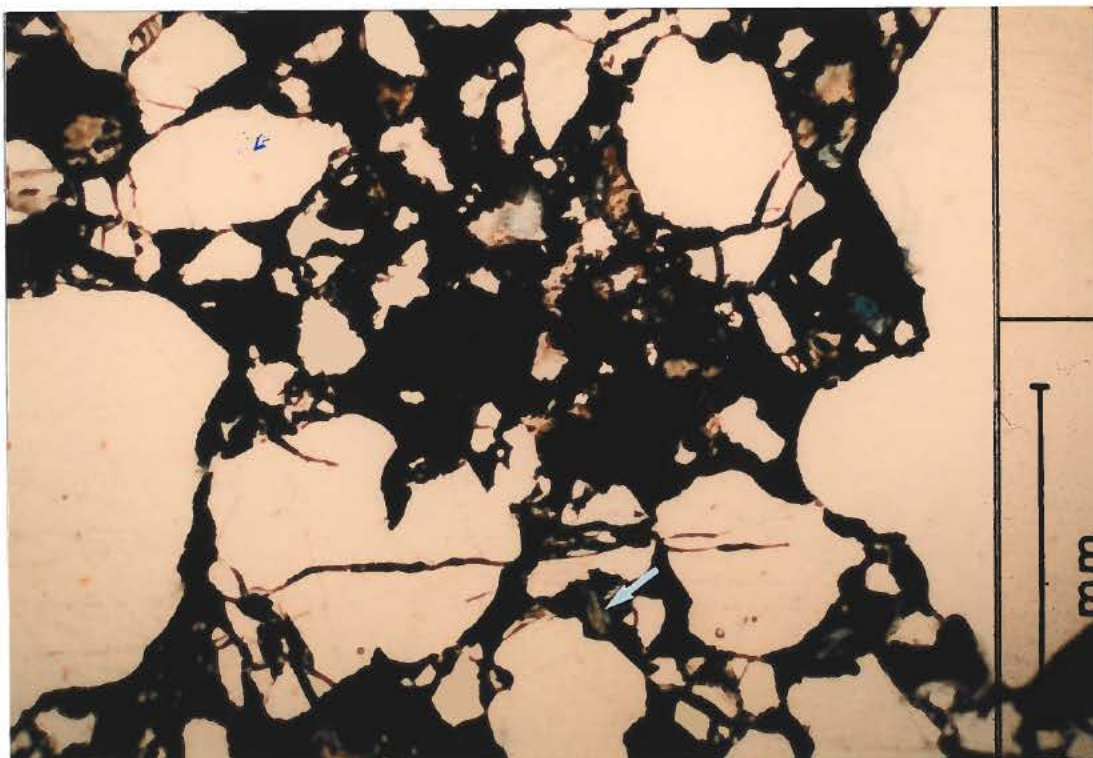


2

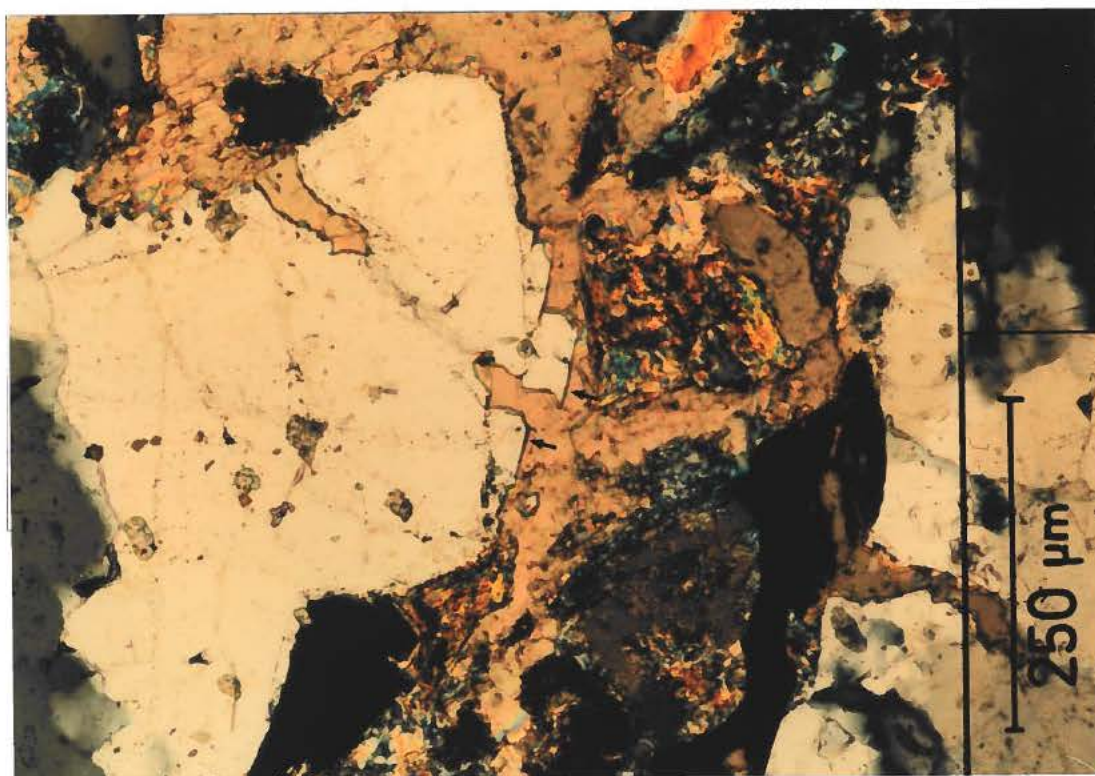


1. Third generation quartz within secondary porosity. Note that the secondary pores are isolated.
2. Overview of porosity (blue) in a post-Campanian sandstone with a permeability near 100mD. Third generation quartz and mixed-layer clay occur in lesser amounts. The distinction between primary and secondary porosity is not straight forward in sandstones with highest permeability.

1



2

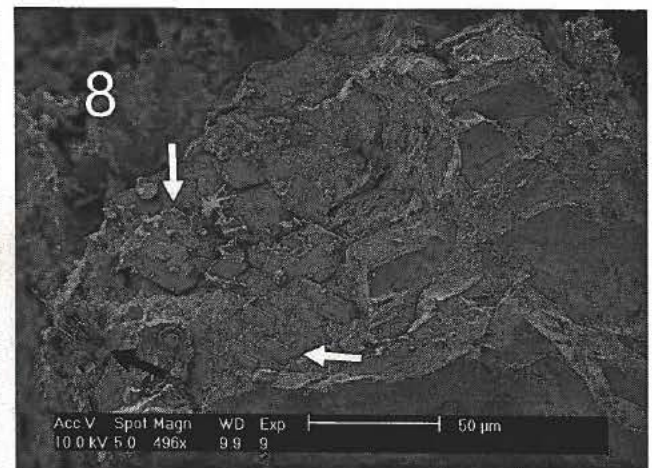
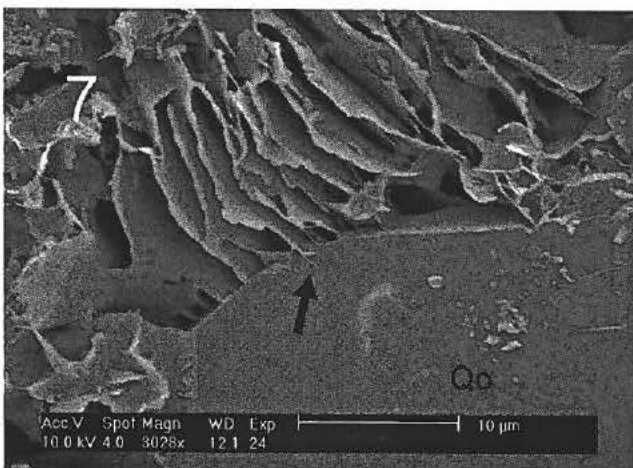
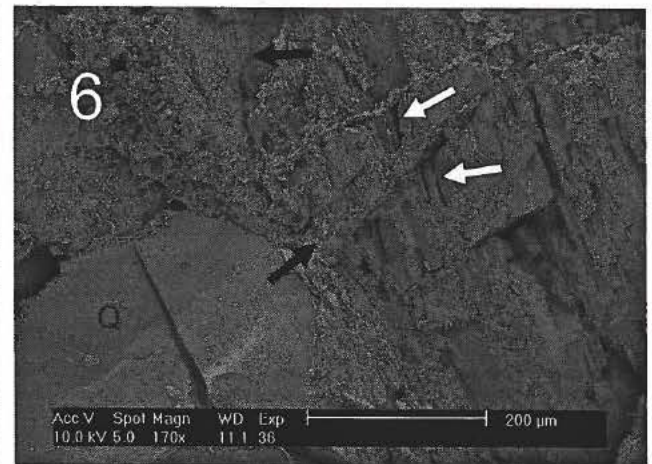
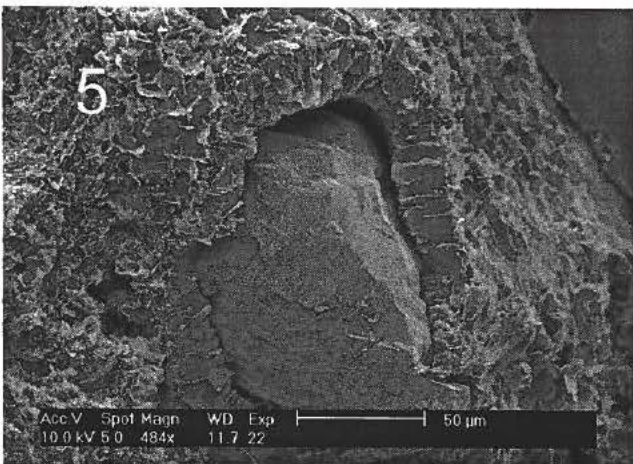
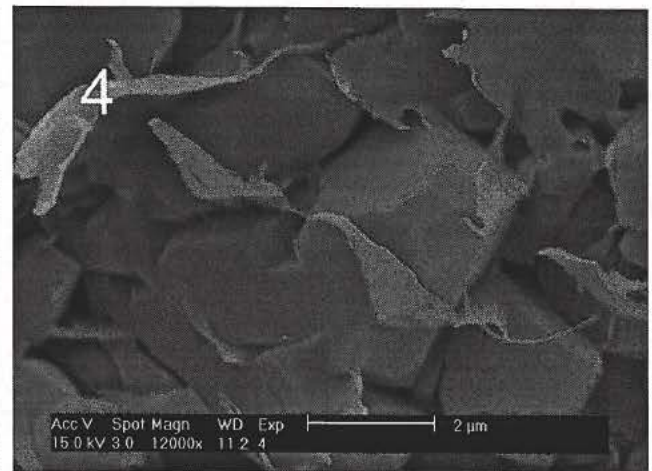
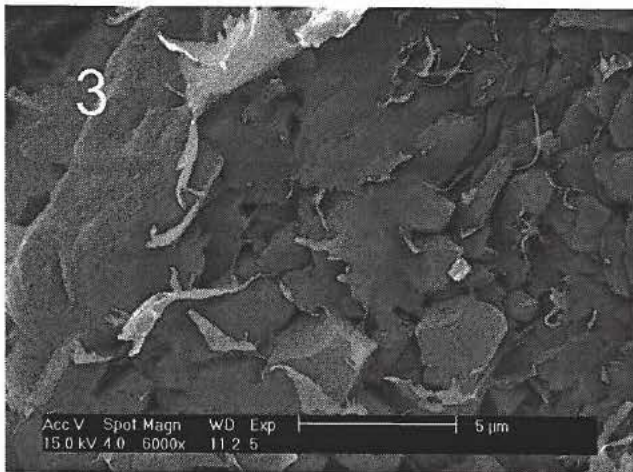
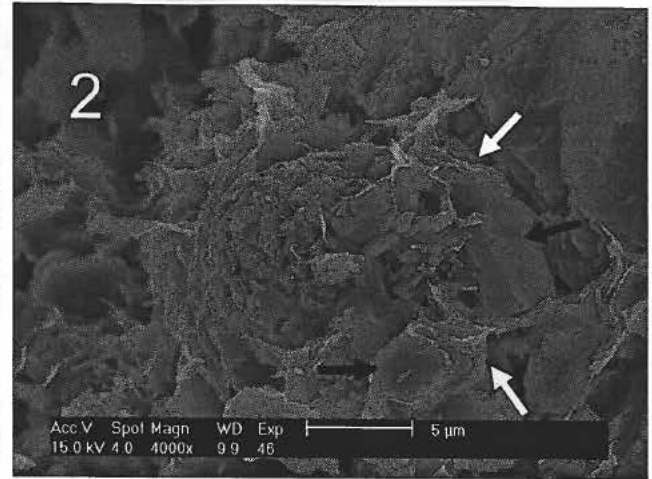
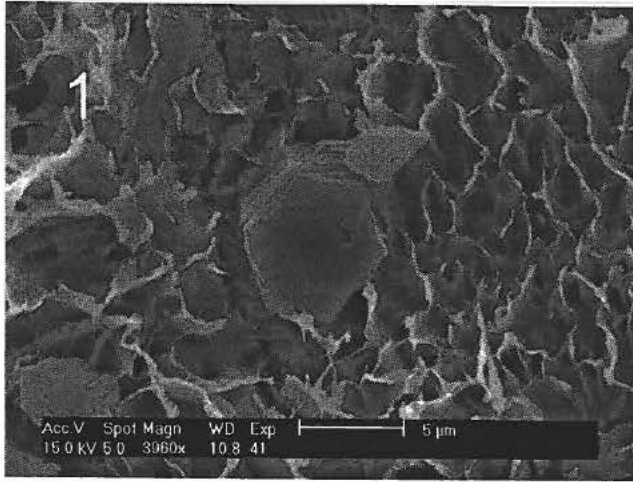


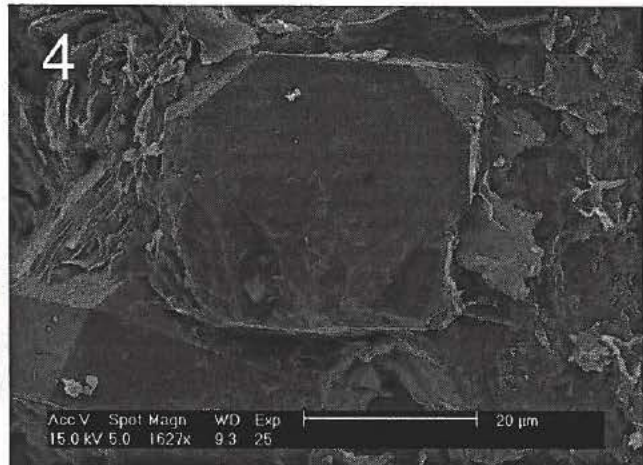
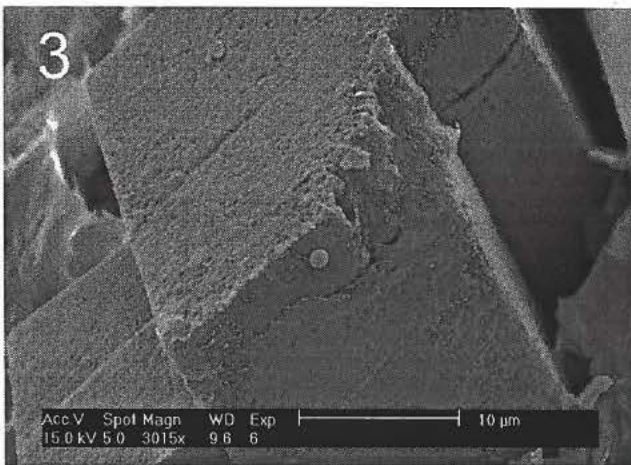
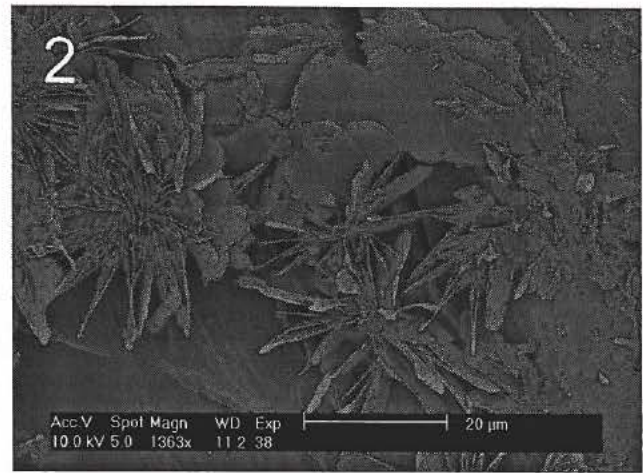
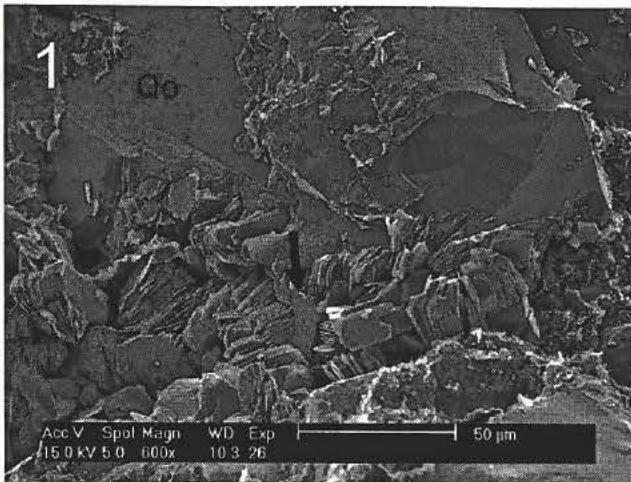
1. Pyrite concretion containing ankerite.

2. Microfracture in detrital quartz grain crosscutting a quartz overgrowth. The fracture is filled with quartz and ankerite suggesting instant healing by quartz.

Scanning electron images

1. Hexagonal apatite crystal elongated along the c-axis.
2. Pyrite framboid and apatite crystal (black arrows) side by side. Mixed-layer clay surrounds the framboid and covers the apatite crystal indicating that mixed-layer clay precipitated after pyrite framboids and apatite.
3. Thin cover of mixed-layer clay on authigenic quartz.
4. Enlargement of quartz crystal shown on Plate 11.3.
5. Thick mixed-layer coating with clay flakes orientated perpendicular to grain surface (sample 134).
6. Mixed-layer clay as coating and fracture fill (black arrow). The quartz grain is fractured during preparation. Elongated dissolution voids occur next to fracture fillings within the feldspar grain indicating some dissolution after precipitation of the mixed-layer clay (sample 134).
7. Authigenic mixed-layer clay caught by 3rd generation quartz (Qo).
8. Partly dissolved potassium feldspar grain where a chlorite fan (black arrow) and albite crystals (white arrows) have nucleated on the dissolution surface.





Scanning electron images

1. Kaolinite booklets surrounded by third generation quartz (Qo). Note the penetration of quartz into the kaolinite aggregate (arrow).
2. Chlorite rosettes (enlargement of Plate 11.6).
3. Euhedral ankerite which is slightly corroded.
4. Pyrite cube near concretionary pyrite.

Back-scatter images of polished thin sections

1. Microcrystalline siderite aggregates. P: porosity, A: ankerite, Q: quartz. See also Plate 4.2.
2. Enlargement of Plate 13.1. Discrete occurrence of Mg-siderite crystals within a darker Al-silicate matrix. Dot indicates point of EDX measurement (analysis 3 in Table xx).
3. Enlargement of Plate 13.1. The quartz has euhedral outlines and is thus authigenic. Remnants of potassium feldspar (K) are present within authigenic quartz indicating growth of quartz and ankerite in a mould of a dissolved feldspar grain.
4. Enlargement of Plate 13.1. Finely crystalline Mg-siderite (type 3) which is paler than microcrystalline siderite (type 1). Dot indicates point of EDX measurement (analysis 2 in Table xx).
5. Overview of a densely packed siderite aggregate. See also Plate 5.1.
6. Enlargement of Plate 13.5.
7. Finely crystalline Mg-siderite (type 3) precipitated (in the contact) between a potassium feldspar grain and a microcrystalline siderite aggregate (type 1). Al: albite, S: siderite (type 3) Dot indicates point of EDX measurement (analysis 4 in Table xx).
8. Microcrystalline Mg-siderite crystals (type 2) within biotite. Note that the crystal does not occur in the porosity between biotite sheets. Finely crystalline siderite (type 3) occurs next to albite in a grain mould.

